A Comparative Assessment of Different Lens Geometries for the Material-by-Design Synthesis of Conformal Arrays

M. Salucci, G. Oliveri, N. Anselmi, and A. Massa

Abstract

In this work, the conformal transformation of linear antenna arrays is dealt with. An innovative Material-by-Design (*MbD*) approach is proposed in order to match a user-defined reference array onto an arbitrary conformal hosting surface without changing its radiating features. Towards this end, a two-step quasi-conformal transformation optics (*QCTO*) methodology is suitably customized and applied to synthesize a meta-material covering of the conformal geometry able to restore the desired radiation characteristics. A comparative assessment between several choices of the lens geometry is given by means of numerical full-wave simulations.

1 "Circular Arc" Geometry - $N' = 20$

1.1 Validation vs. Lens Curvature (l) and Lens Thickness (s)

Input Parameters

- **Virtual & Physical Geometries**

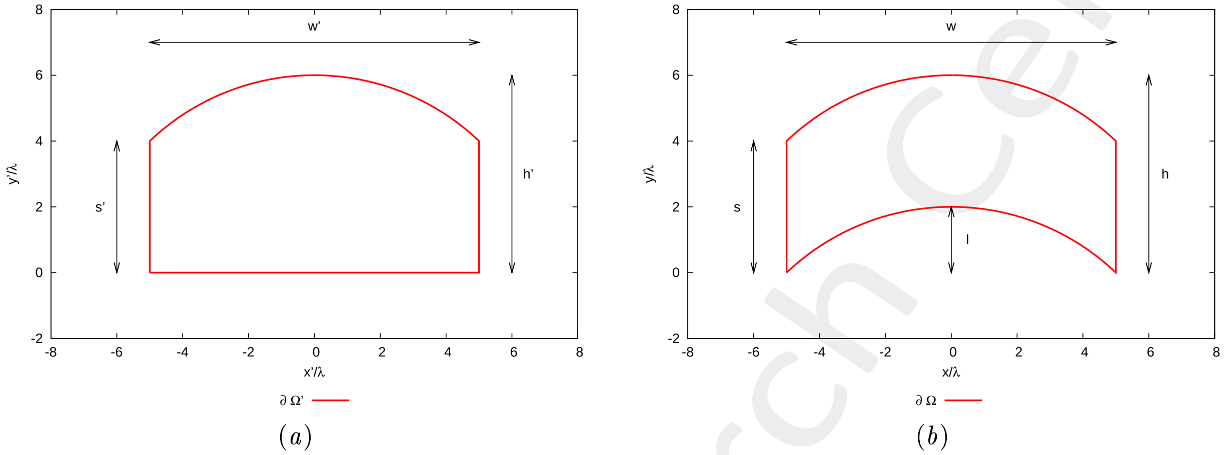

Figure 1: Transformation regions and geometric parameters of interest.

Lens Thickness: $s = 4.0$ [λ]						
Virtual			**Physical**			
w' [λ]	h' [λ]	s' [λ]	w [λ]	h [λ]	s [λ]	l [λ] (Curvature)
16.0	4.5	4.0	16.0	4.5	4.0	**0.5**
16.0	5.0	4.0	16.0	5.0	4.0	**1.0**
16.0	5.5	4.0	16.0	5.5	4.0	**1.5**
16.0	6.0	4.0	16.0	6.0	4.0	**2.0**

Lens Thickness: $s = 2.0$ [λ]						
Virtual			**Physical**			
w' [λ]	h' [λ]	s' [λ]	w [λ]	h [λ]	s [λ]	l [λ] (Curvature)
16.0	2.5	2.0	16.0	2.5	2.0	**0.5**
16.0	3.0	2.0	16.0	3.0	2.0	**1.0**
16.0	3.5	2.0	16.0	3.5	2.0	**1.5**
16.0	4.0	2.0	16.0	4.0	2.0	**2.0**

Lens Thickness: $s = 1.0$ [λ]						
Virtual			**Physical**			
w' [λ]	h' [λ]	s' [λ]	w [λ]	h [λ]	s [λ]	l [λ] (Curvature)
16.0	1.5	1.0	16.0	1.5	1.0	**0.5**
16.0	2.0	1.0	16.0	2.0	1.0	**1.0**
16.0	2.5	1.0	16.0	2.5	1.0	**1.5**
16.0	3.0	1.0	16.0	3.0	1.0	**2.0**

Lens Thickness: $s = 0.5$ [λ]						
Virtual			**Physical**			
w' [λ]	h' [λ]	s' [λ]	w [λ]	h [λ]	s [λ]	l [λ] (Curvature)
16.0	1.0	0.5	16.0	1.0	0.5	**0.5**
16.0	1.5	0.5	16.0	1.5	0.5	**1.0**
16.0	2.0	0.5	16.0	2.0	0.5	**1.5**
16.0	2.5	0.5	16.0	2.5	0.5	**2.0**

Table I: Geometric descriptors for virtual and physical geometries. Note that $w' = w$, $h' = h$, $s' = s$, and $h = s + l$.

- **Virtual Array**
  - Number of elements, spacing, aperture: $N' = 20$, $d' = \frac{\lambda}{2}$, $L' = 9.5$ $[\lambda]$;
  - Distance from PEC ground plane (placed at $y' = 0.0$): $\delta' = \frac{\lambda}{4}$;
  - Operating frequency: $f = 600$ $[MHz]$;
  - Steering angle: $\phi_s = 90.0$ $[deg]$;
  - Excitations: $I_n = 1.0$, $\varphi_n = \frac{-2\pi}{\lambda} x_n sin\left(\phi_s + 90\right)$; $n = 1, ..., N'$;
- **QCTO**
  - Discretization cell dimension: 0.15 $[\lambda]$ (0.01 $[\lambda]$ for source mapping);

1.1.1 Results of the Transformation

Lens Thickness $s = 4.0$ $[\lambda]$

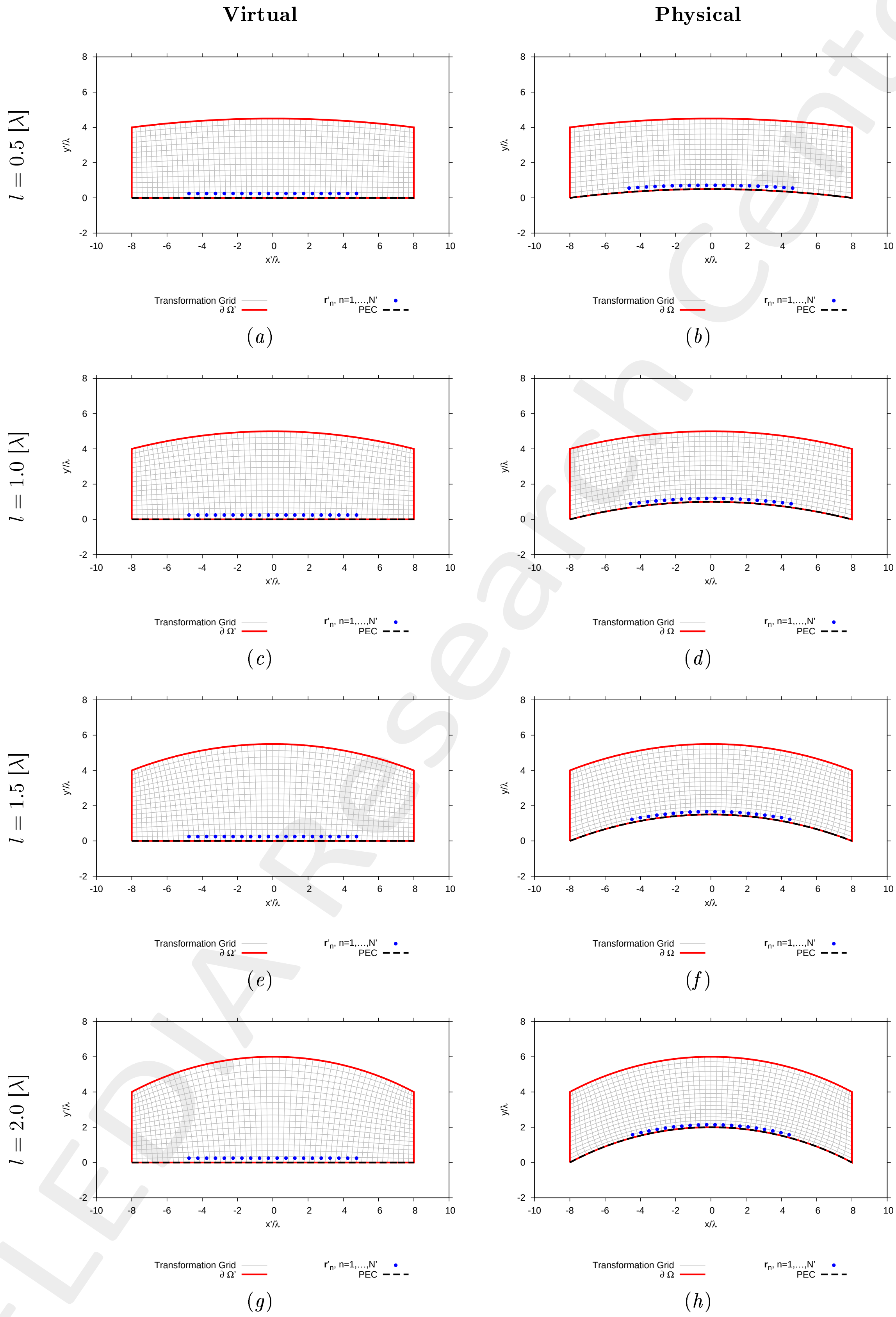

Figure 2: Lens thickness $s = 4.0$ $[\lambda]$ - Transformation grids for virtual and physical geometries for different curvatures of the lens.

Lens Thickness $s = 2.0$ [λ]

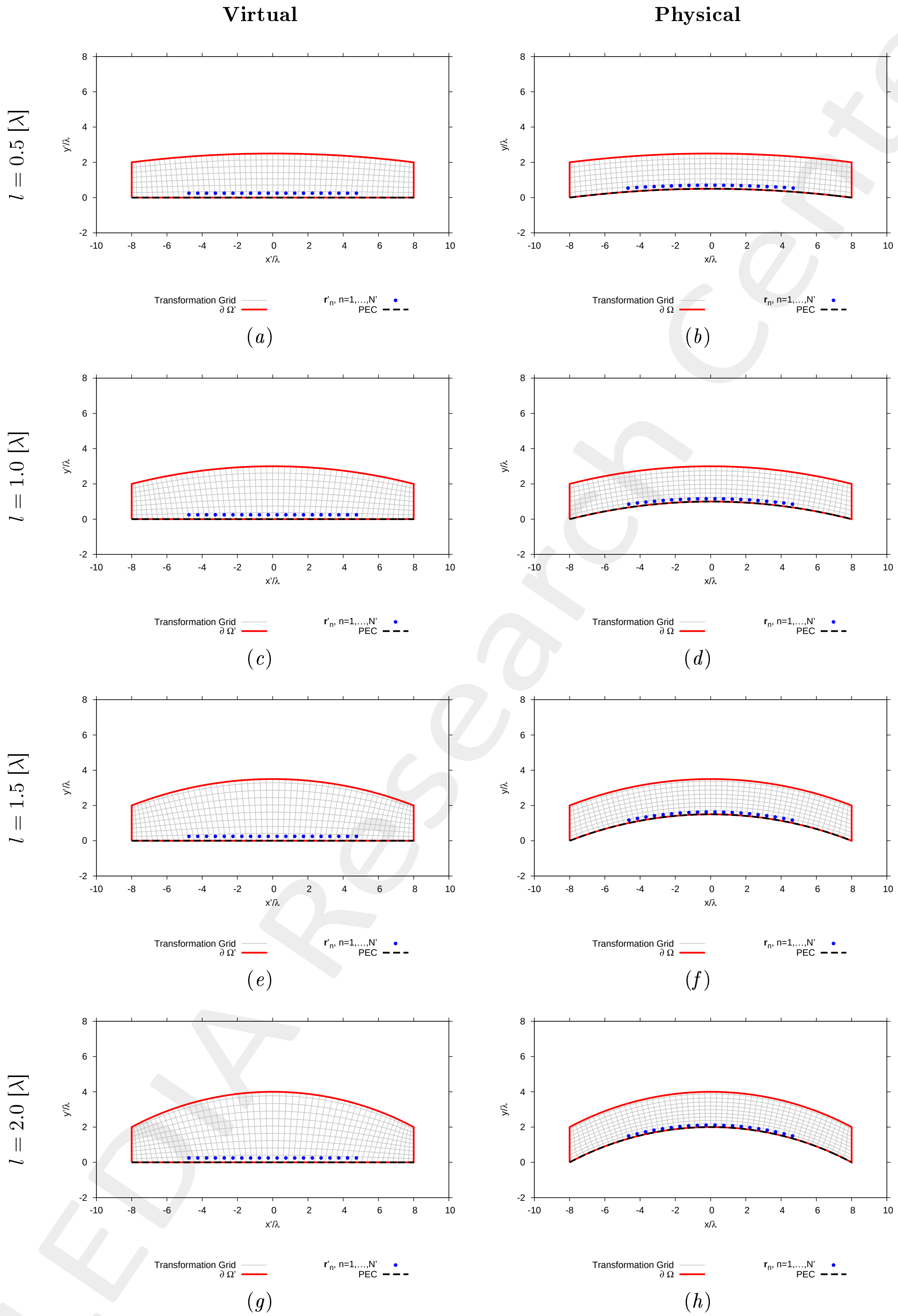

Figure 3: Lens thickness $s = 2.0$ [λ] - Transformation grids for virtual and physical geometries for different curvatures of the lens.

Lens Thickness $s = 1.0$ [λ]

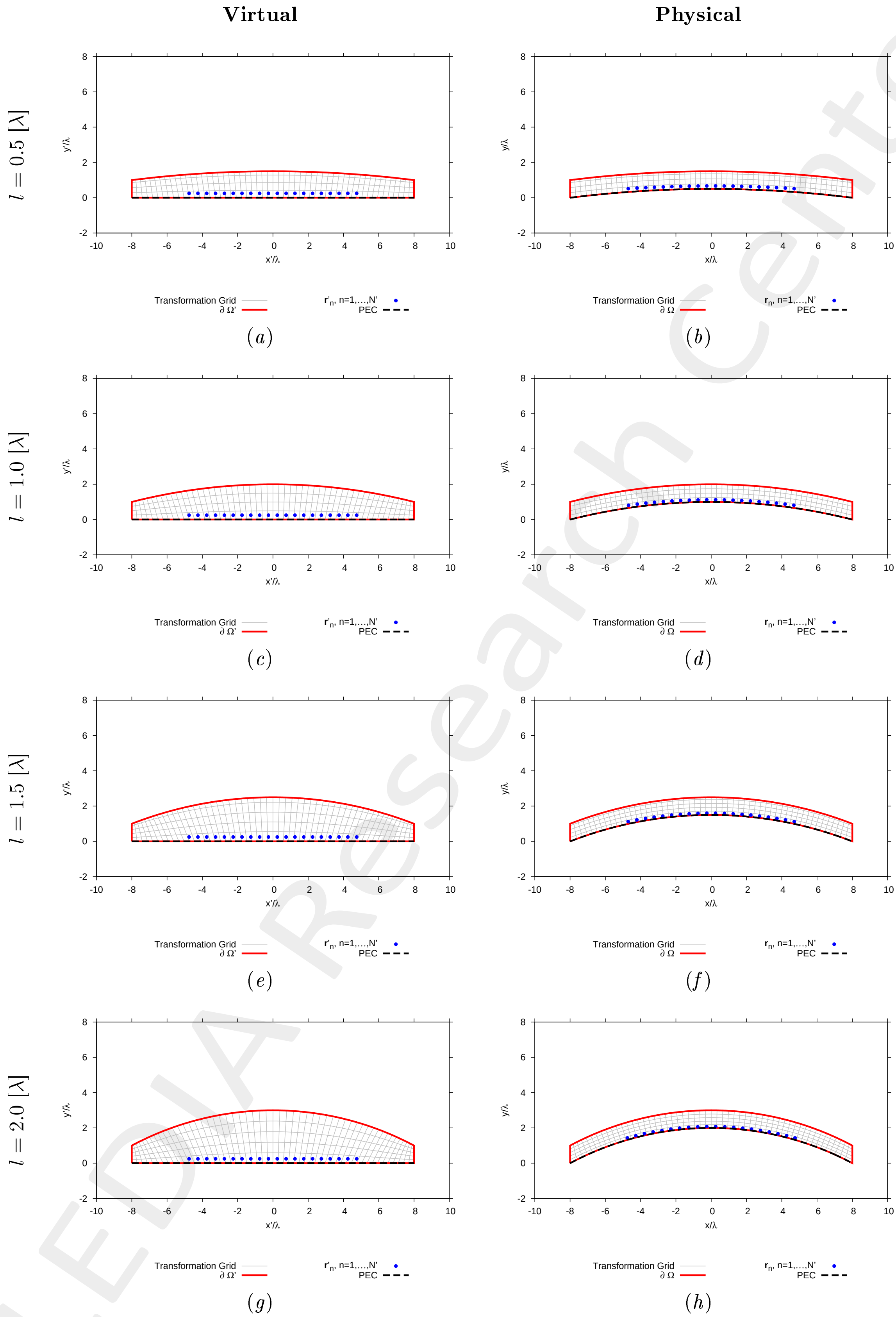

Figure 4: Lens thickness $s = 1.0$ [λ] - Transformation grids for virtual and physical geometries for different curvatures of the lens.

Lens Thickness $s = 0.5$ [λ]

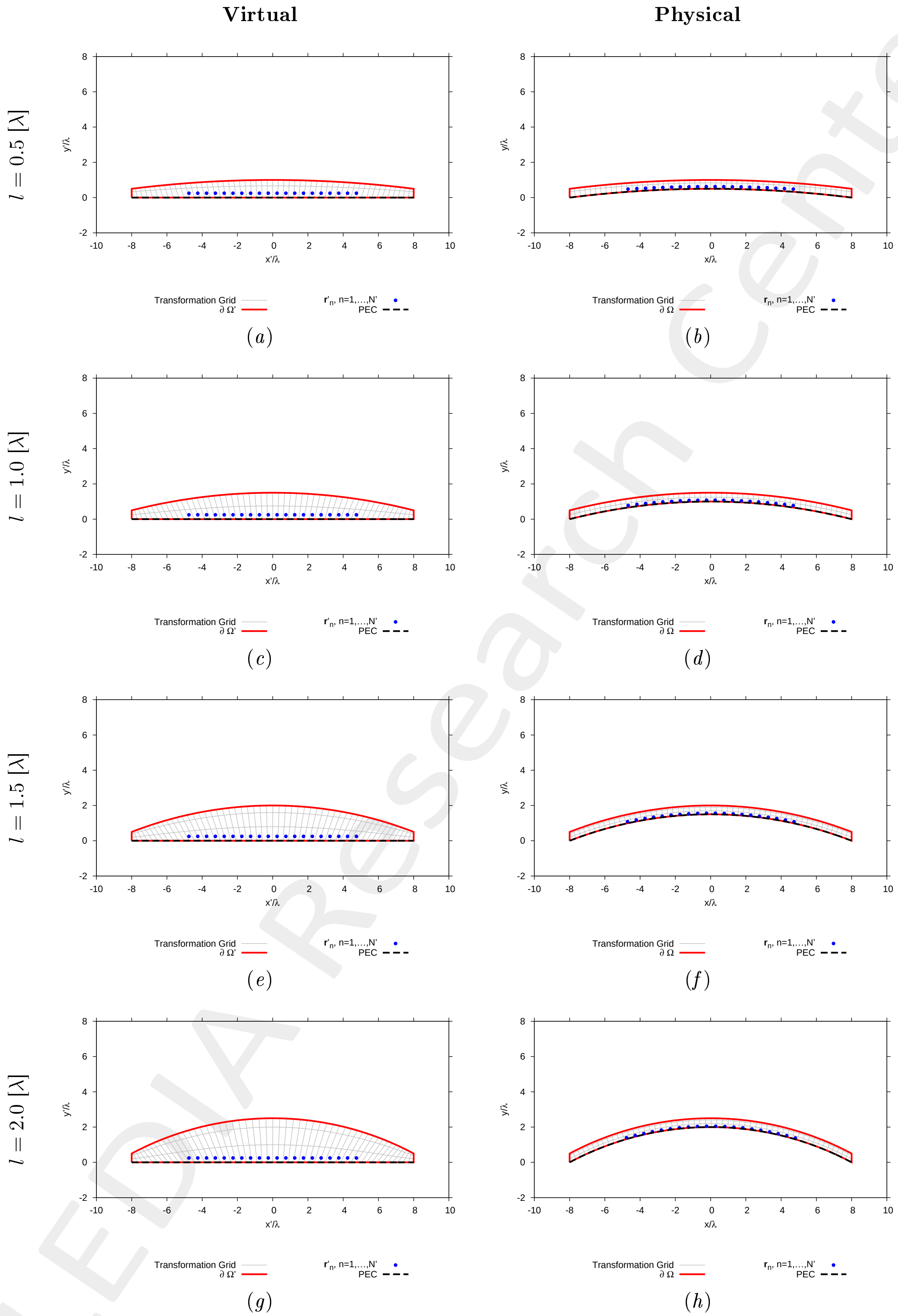

Figure 5: Lens thickness $s = 0.5$ [λ] - Transformation grids for virtual and physical geometries for different curvatures of the lens.

1.1.2 Physical Lens Parameters

Lens Curvature $l = 0.5$ $[\lambda]$				
	$s = 4.0$ $[\lambda]$	$s = 2.0$ $[\lambda]$	$s = 1.0$ $[\lambda]$	$s = 0.5$ $[\lambda]$
Anisotropic Permittivity Range	$[-0.110, 1.280]$	$[-0.110, 1.290]$	$[-0.220, 1.560]$	$[-0.390, 2.070]$
Isotropic Permittivity Range	$[0.00, 1.230]$	$[0.00, 1.190]$	$[0.00, 1.150]$	$[0.00, 1.150]$
Lens Curvature $l = 1.0$ $[\lambda]$				
	$s = 4.0$ $[\lambda]$	$s = 2.0$ $[\lambda]$	$s = 1.0$ $[\lambda]$	$s = 0.5$ $[\lambda]$
Anisotropic Permittivity Range	$[-0.280, 1.690]$	$[-0.260, 1.590]$	$[-0.450, 2.150]$	$[-0.780, 3.220]$
Isotropic Permittivity Range	$[0.00, 1.500]$	$[0.00, 1.410]$	$[0.00, 1.310]$	$[0.00, 1.310]$
Lens Curvature $l = 1.5$ $[\lambda]$				
	$s = 4.0$ $[\lambda]$	$s = 2.0$ $[\lambda]$	$s = 1.0$ $[\lambda]$	$s = 0.5$ $[\lambda]$
Anisotropic Permittivity Range	$[-0.620, 2.170]$	$[-0.540, 1.980]$	$[-0.710, 2.760]$	$[-1.240, 4.420]$
Isotropic Permittivity Range	$[0.00, 1.800]$	$[0.00, 1.640]$	$[0.00, 1.450]$	$[0.00, 1.500]$
Lens Curvature $l = 2.0$ $[\lambda]$				
	$s = 4.0$ $[\lambda]$	$s = 2.0$ $[\lambda]$	$s = 1.0$ $[\lambda]$	$s = 0.5$ $[\lambda]$
Anisotropic Permittivity Range	$[-1.150, 2.750]$	$[-0.980, 2.440]$	$[-1.020, 3.350]$	$[-1.790, 5.640]$
Isotropic Permittivity Range	$[0.00, 2.090]$	$[0.00, 1.850]$	$[0.00, 1.590]$	$[0.00, 1.660]$

Table II: Permittivity ranges of the physical lens.

1.1.3 Far-Field Patterns (Aniso-Lens, $\phi_s = 90.0$ $[deg]$)

Lens Thickness $s = 4.0$ $[\lambda]$

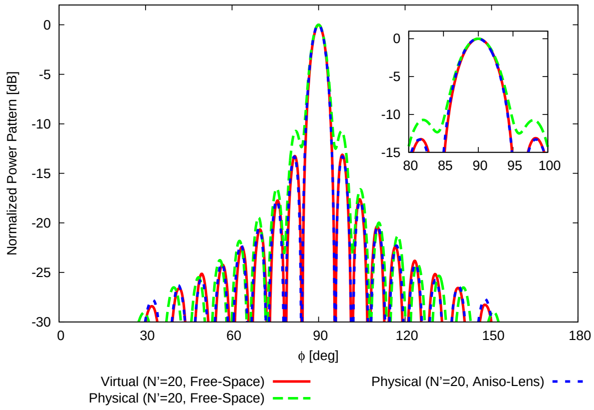

(a) $l = 0.5$ $[\lambda]$

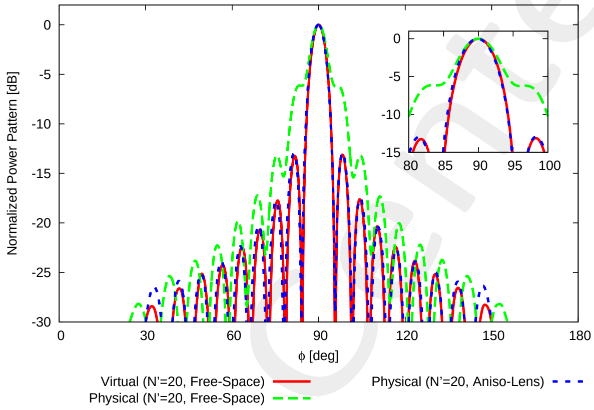

(b) $l = 1.0$ $[\lambda]$

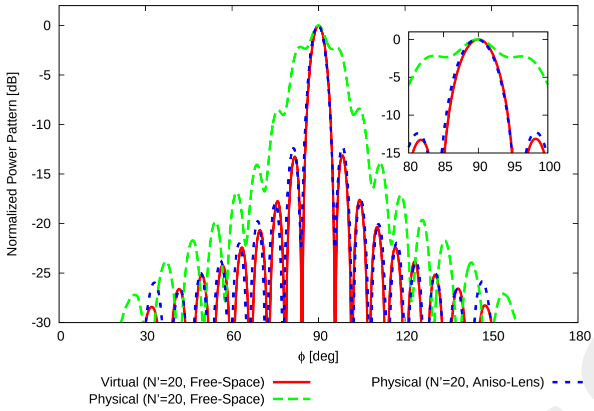

(c) $l = 1.5$ $[\lambda]$

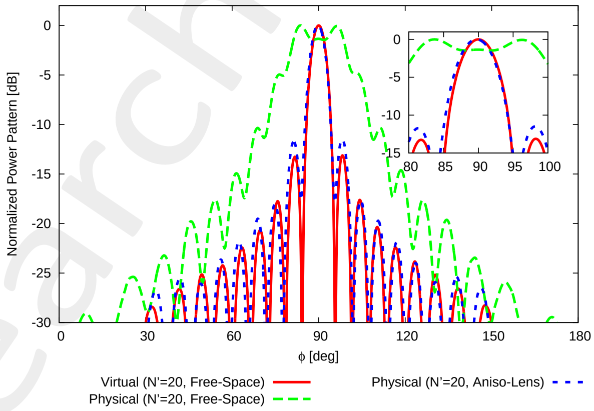

(d) $l = 2.0$ $[\lambda]$

Figure 6: Lens thickness $s = 4.0$ $[\lambda]$ - Comparison between the far field patterns or different curvatures of the lens.

Lens Thickness $s = 2.0$ $[\lambda]$

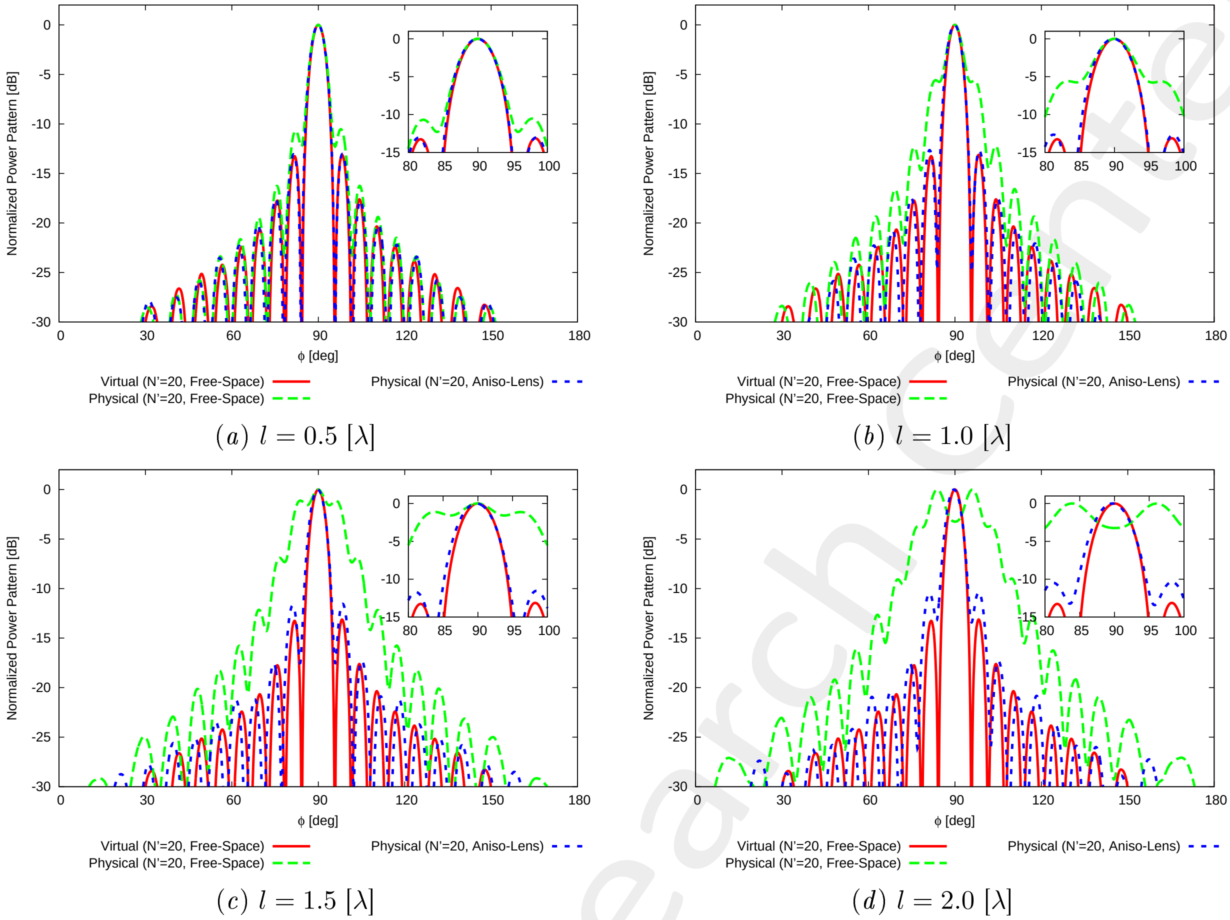

Figure 7: Lens thickness $s = 2.0$ $[\lambda]$ - Comparison between the far field patterns or different curvatures of the lens.

Lens Thickness $s = 1.0$ **[**λ**]**

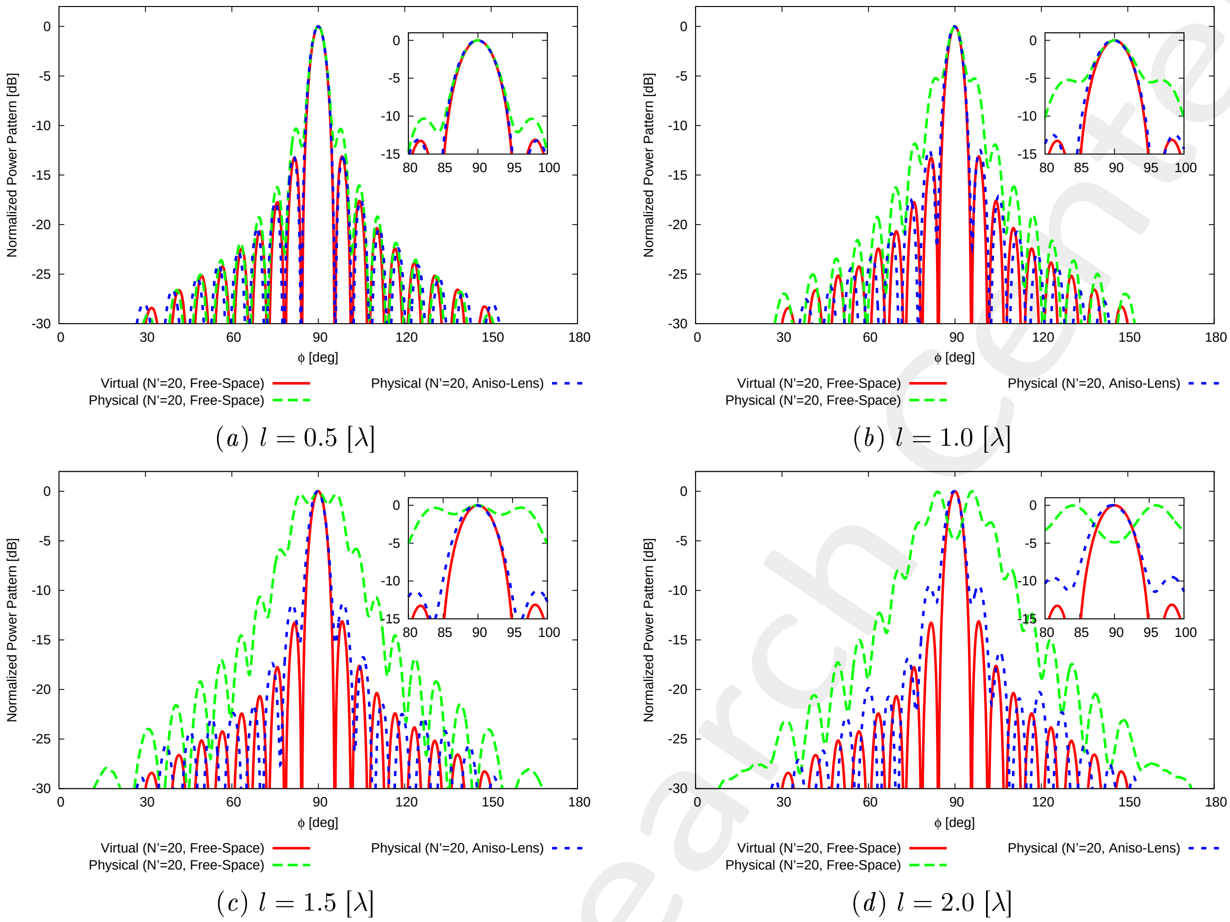

Figure 8: Lens thickness $s = 1.0$ $[\lambda]$ - Comparison between the far field patterns or different curvatures of the lens.

Lens Thickness $s = 0.5$ $[\lambda]$

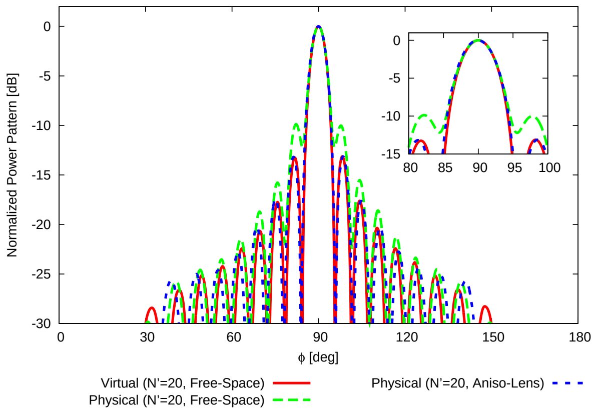

(a) $l = 0.5$ $[\lambda]$

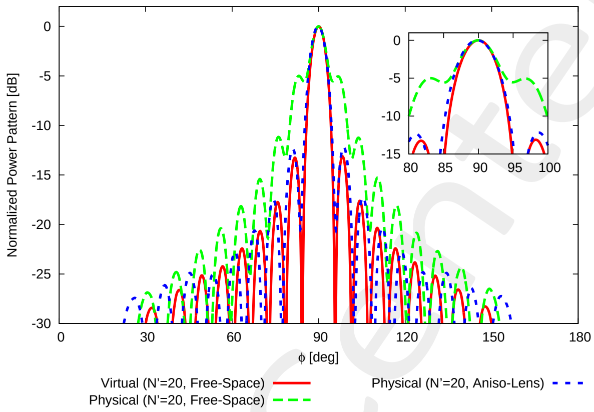

(b) $l = 1.0$ $[\lambda]$

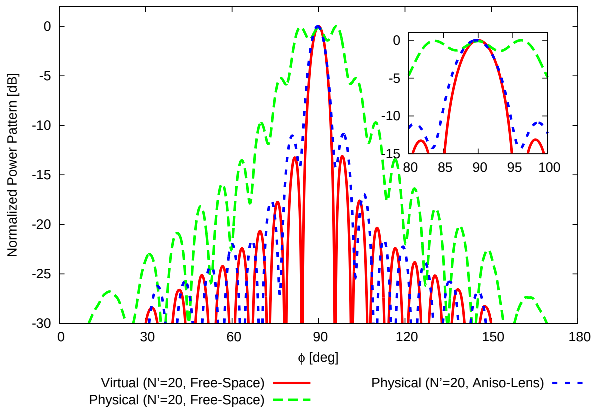

(c) $l = 1.5$ $[\lambda]$

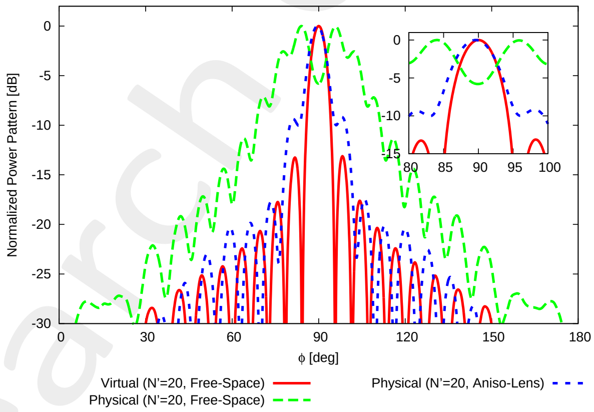

(d) $l = 2.0$ $[\lambda]$

Figure 9: Lens thickness $s = 0.5$ $[\lambda]$ - Comparison between the far field patterns or different curvatures of the lens.

Observations

- Increasing the curvature ($\uparrow l$) leads to a worsening of the performances;
- Decreasing the lens thickness ($\downarrow s$) leads to a worsening of the performances;
- The thinner the lens, the fastest the degradation w.r.t. the curvature.

1.2 Final Resume

1.2.1 Pattern Performances vs. Lens Curvature (l)

Before SI ($\phi_s = 90$ [deg], $f = 600$[MHz])

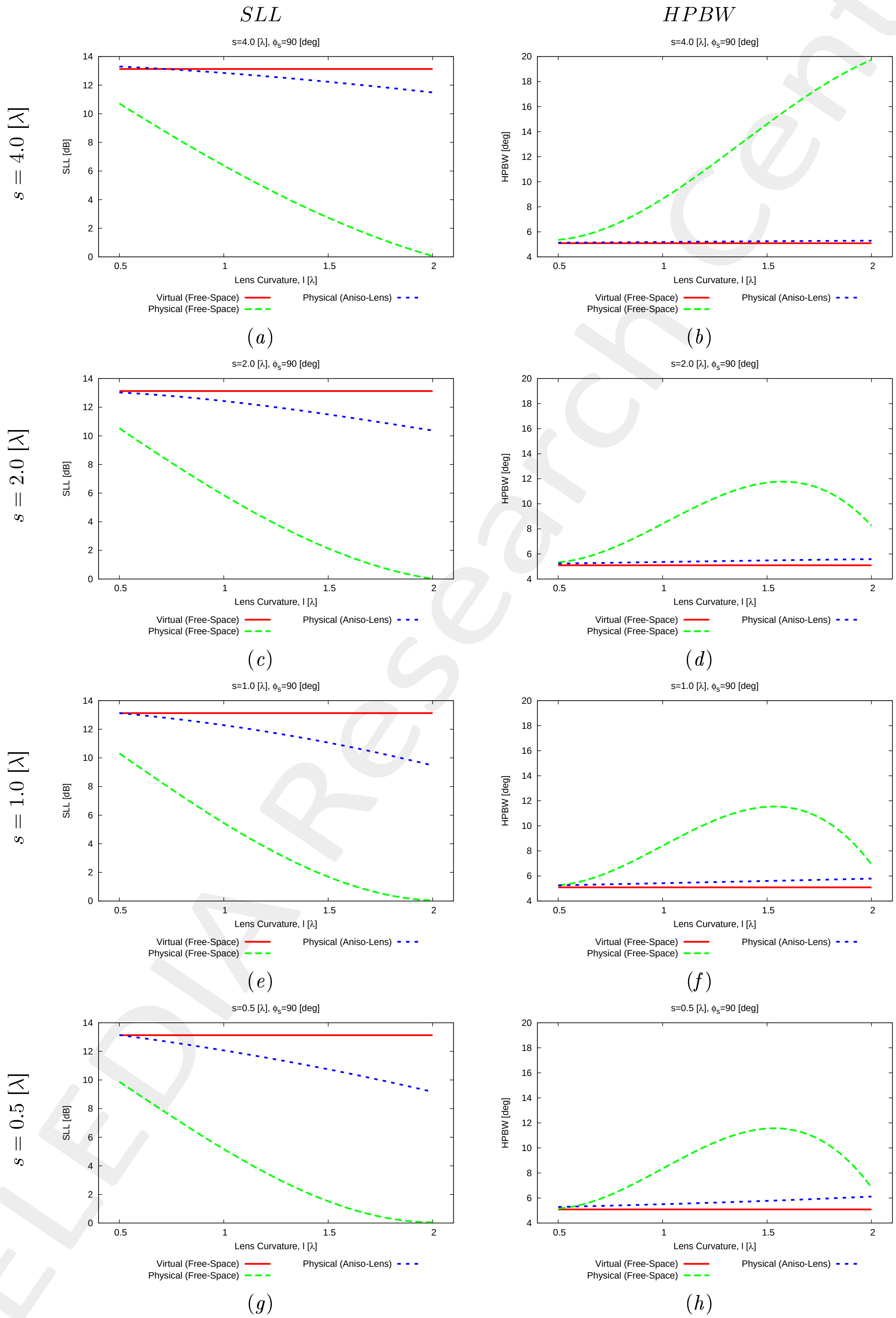

Figure 10: $\phi_s = 90$ [deg], $f = 600$[MHz] - SLL and $HPBW$ vs. the lens curvature (l).

1.2.2 Pattern Performances vs. Lens Thickness (s)

Before SI ($\phi_s = 90$ [deg], $f = 600$[MHz])

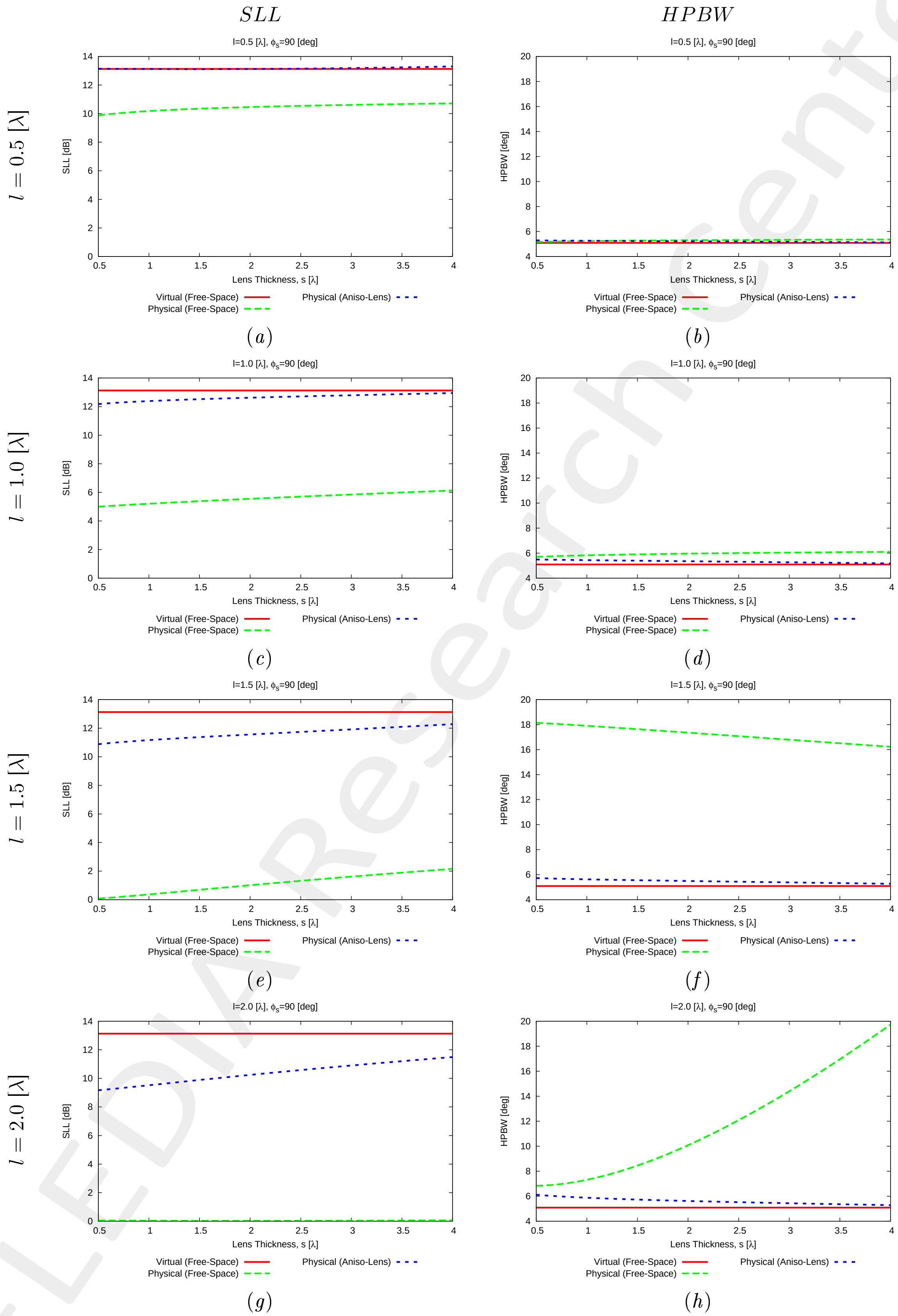

Figure 11: $\phi_s = 90$ [deg], $f = 600$[MHz] - SLL and $HPBW$ vs. the lens thickness (s).

1.2.3 Pattern Performances vs. Lens Curvature (l) and vs. Lens Thickness (s)

Before SI ($\phi_s = 90$ [deg], $f = 600$[MHz] - Physical Array (Aniso-Lens))

Characteristics of the virtual array ($N' = 20$, Free-Space)

- $SLL = 13.13$ [dB];
- $FNBW = 11.44$ [deg];
- $HPBW = 5.09$ [deg];

SLL $HPBW$

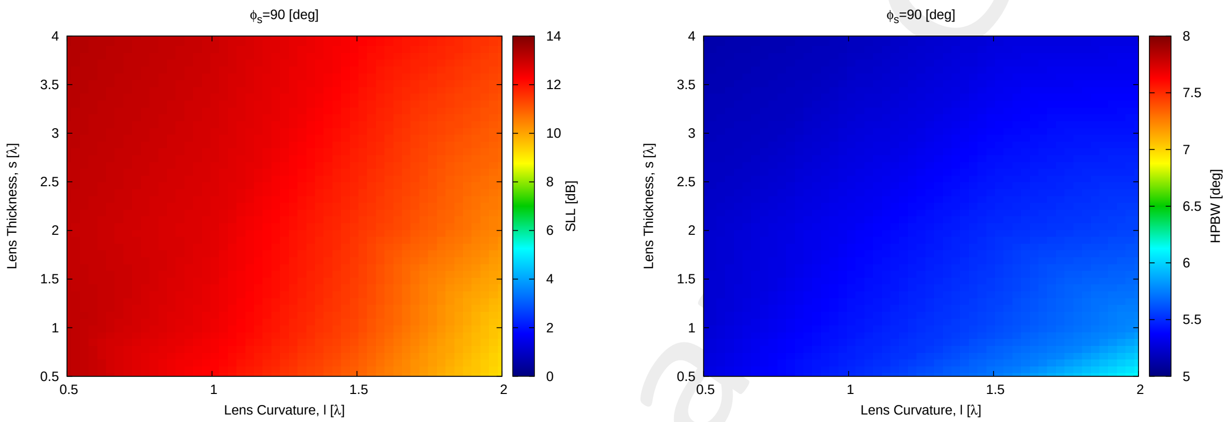

(a) (b)

Figure 12: $\phi_s = 90$ [deg], $f = 600$[MHz] - SLL and $HPBW$ vs. the lens thickness (s) and the lens curvature (l).

2 "Gaussian Bridge" Geometry - $N' = 20$

2.1 Validation vs. Lens Curvature (l) and Lens Thickness (s)

Input Parameters

- **Virtual & Physical Geometries**

  NOTE: The curved profile is given by a Gaussian function, with standard deviation equal to σ and imposing $w^{'} = 6\sigma$.

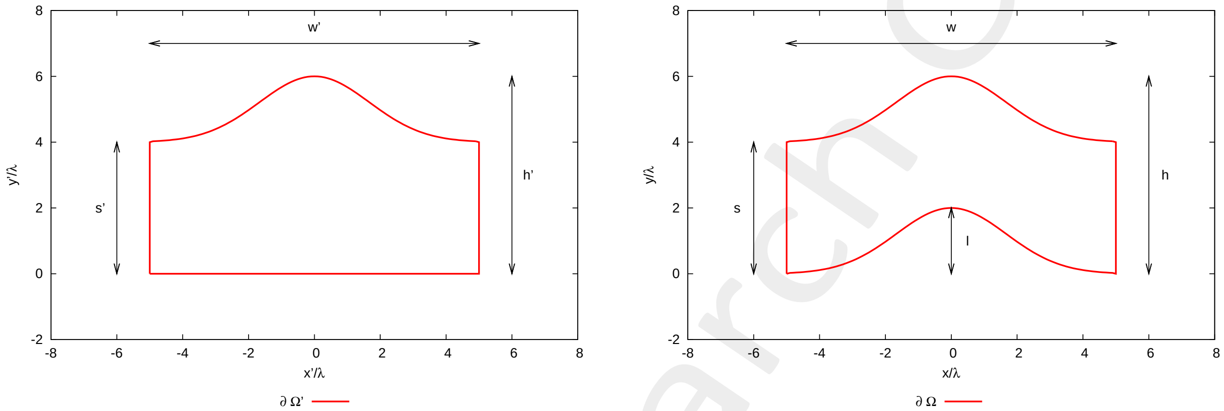

(a) (b)

Figure 13: Transformation regions and geometric parameters of interest.

Lens Thickness: $s = 4.0$ [λ]						
Virtual			**Physical**			
w' [λ]	h' [λ]	s' [λ]	w [λ]	h [λ]	s [λ]	l [λ] (Curvature)
16.0	4.5	4.0	16.0	4.5	4.0	**0.5**
16.0	5.0	4.0	16.0	5.0	4.0	**1.0**
16.0	5.5	4.0	16.0	5.5	4.0	**1.5**
16.0	6.0	4.0	16.0	6.0	4.0	**2.0**
Lens Thickness: $s = 2.0$ [λ]						
Virtual			**Physical**			
w' [λ]	h' [λ]	s' [λ]	w [λ]	h [λ]	s [λ]	l [λ] (Curvature)
16.0	2.5	2.0	16.0	2.5	2.0	**0.5**
16.0	3.0	2.0	16.0	3.0	2.0	**1.0**
16.0	3.5	2.0	16.0	3.5	2.0	**1.5**
16.0	4.0	2.0	16.0	4.0	2.0	**2.0**
Lens Thickness: $s = 1.0$ [λ]						
Virtual			**Physical**			
w' [λ]	h' [λ]	s' [λ]	w [λ]	h [λ]	s [λ]	l [λ] (Curvature)
16.0	1.5	1.0	16.0	1.5	1.0	**0.5**
16.0	2.0	1.0	16.0	2.0	1.0	**1.0**
16.0	2.5	1.0	16.0	2.5	1.0	**1.5**
16.0	3.0	1.0	16.0	3.0	1.0	**2.0**
Lens Thickness: $s = 0.5$ [λ]						
Virtual			**Physical**			
w' [λ]	h' [λ]	s' [λ]	w [λ]	h [λ]	s [λ]	l [λ] (Curvature)
16.0	1.0	0.5	16.0	1.0	0.5	**0.5**
16.0	1.5	0.5	16.0	1.5	0.5	**1.0**
16.0	2.0	0.5	16.0	2.0	0.5	**1.5**
16.0	2.5	0.5	16.0	2.5	0.5	**2.0**

Table III: Geometric descriptors for virtual and physical geometries. Note that $w' = w$, $h' = h$, $s' = s$, and $h = s + l$.

- **Virtual Array**
  - Number of elements, spacing, aperture: $N' = 20$, $d' = \frac{\lambda}{2}$, $L' = 9.5$ [λ];
  - Distance from PEC ground plane (placed at $y' = 0.0$): $\delta' = \frac{\lambda}{4}$;
  - Operating frequency: $f = 600$ $[MHz]$;
  - Steering angle: $\phi_s = 90.0$ $[deg]$;
  - Excitations: $I_n = 1.0$, $\varphi_n = \frac{-2\pi}{\lambda} x_n sin\left(\phi_s + 90\right)$; $n = 1, ..., N'$;
- **QCTO**
  - Discretization cell dimension: 0.15 [λ] (0.01 [λ] for source mapping);

2.1.1 Results of the Transformation

Lens Thickness $s = 4.0$ $[\lambda]$

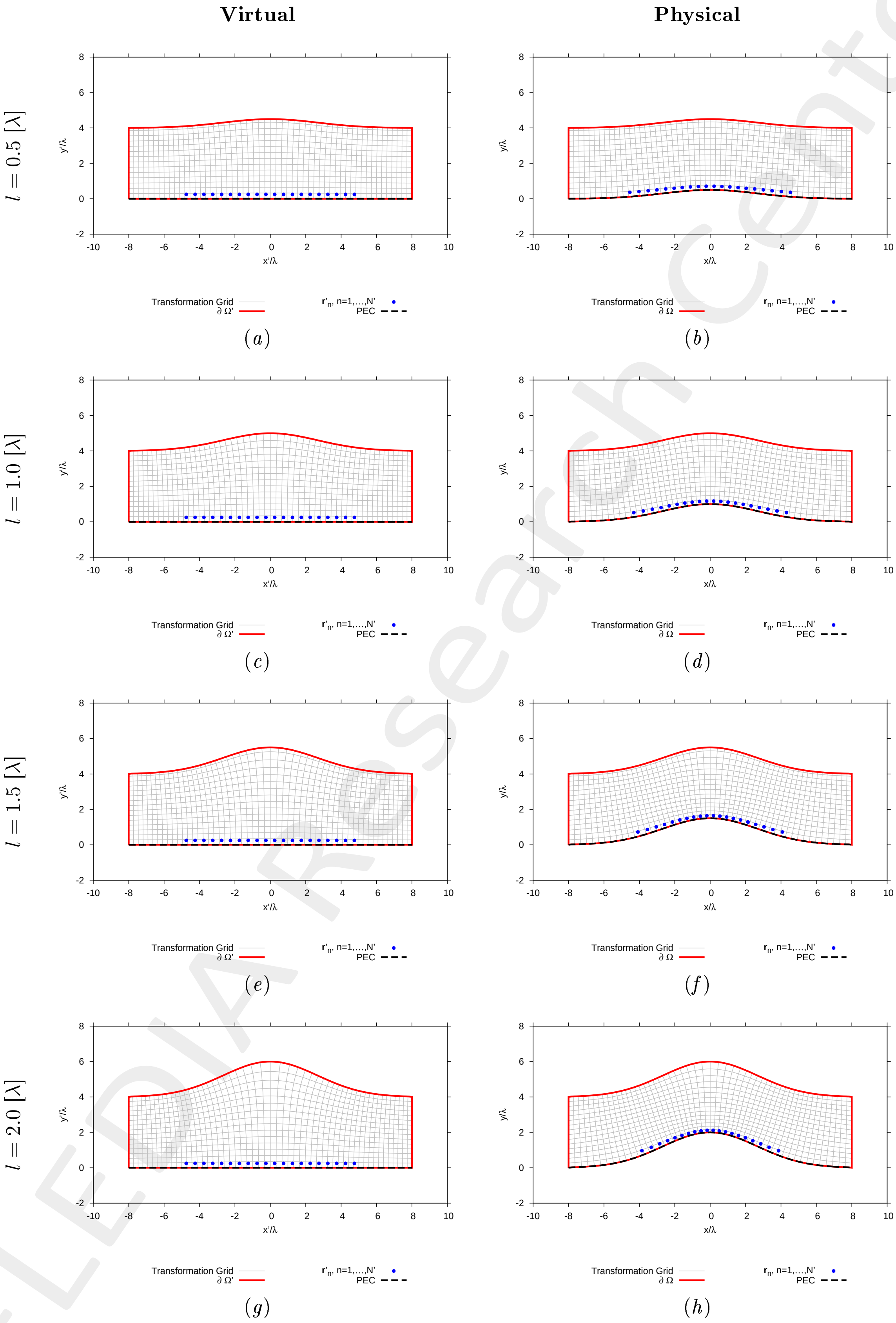

Figure 14: Lens thickness $s = 4.0$ $[\lambda]$ - Transformation grids for virtual and physical geometries for different curvatures of the lens.

Lens Thickness $s = 2.0$ [λ]

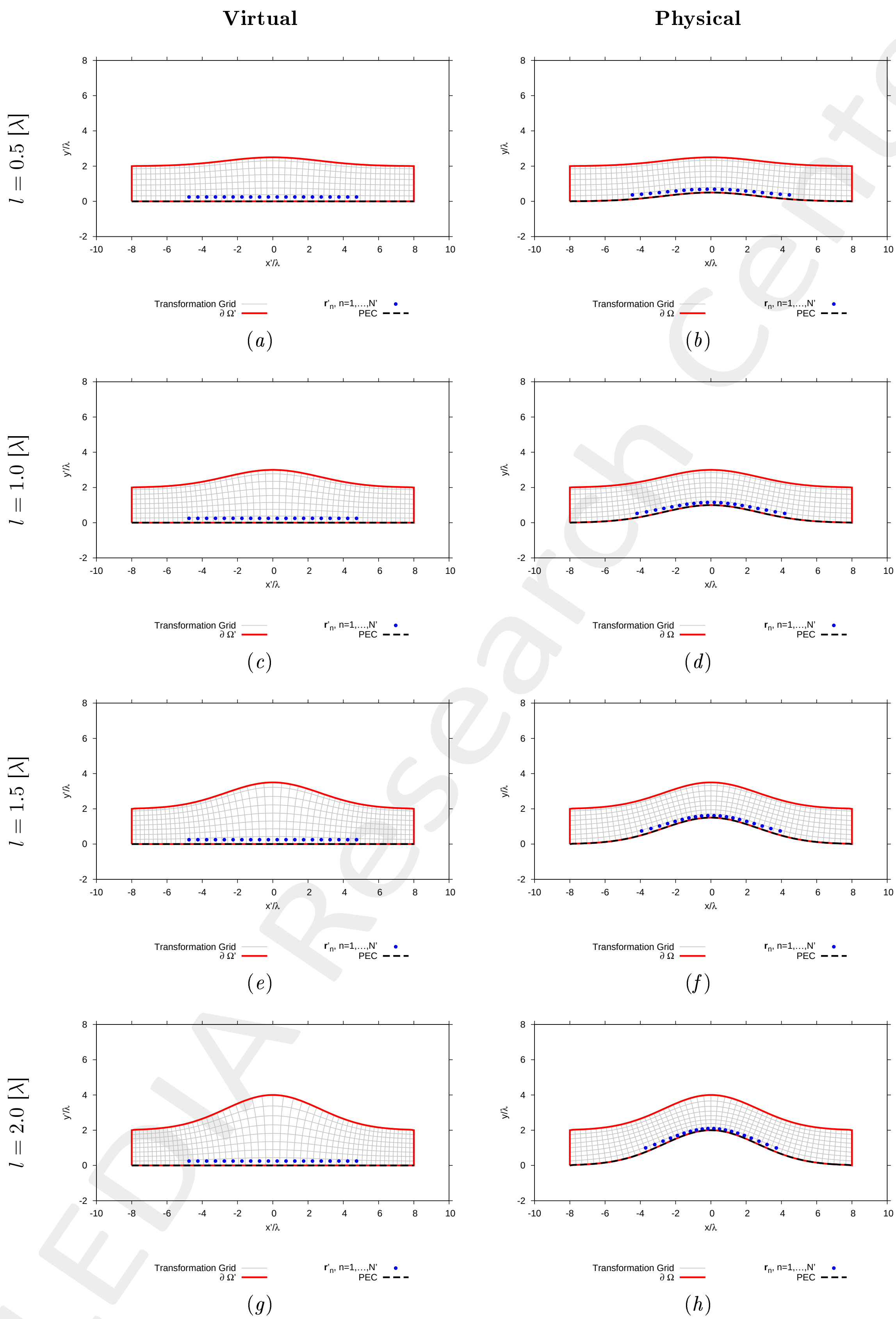

Figure 15: Lens thickness $s = 2.0$ [λ] - Transformation grids for virtual and physical geometries for different curvatures of the lens.

Lens Thickness $s = 1.0$ [λ]

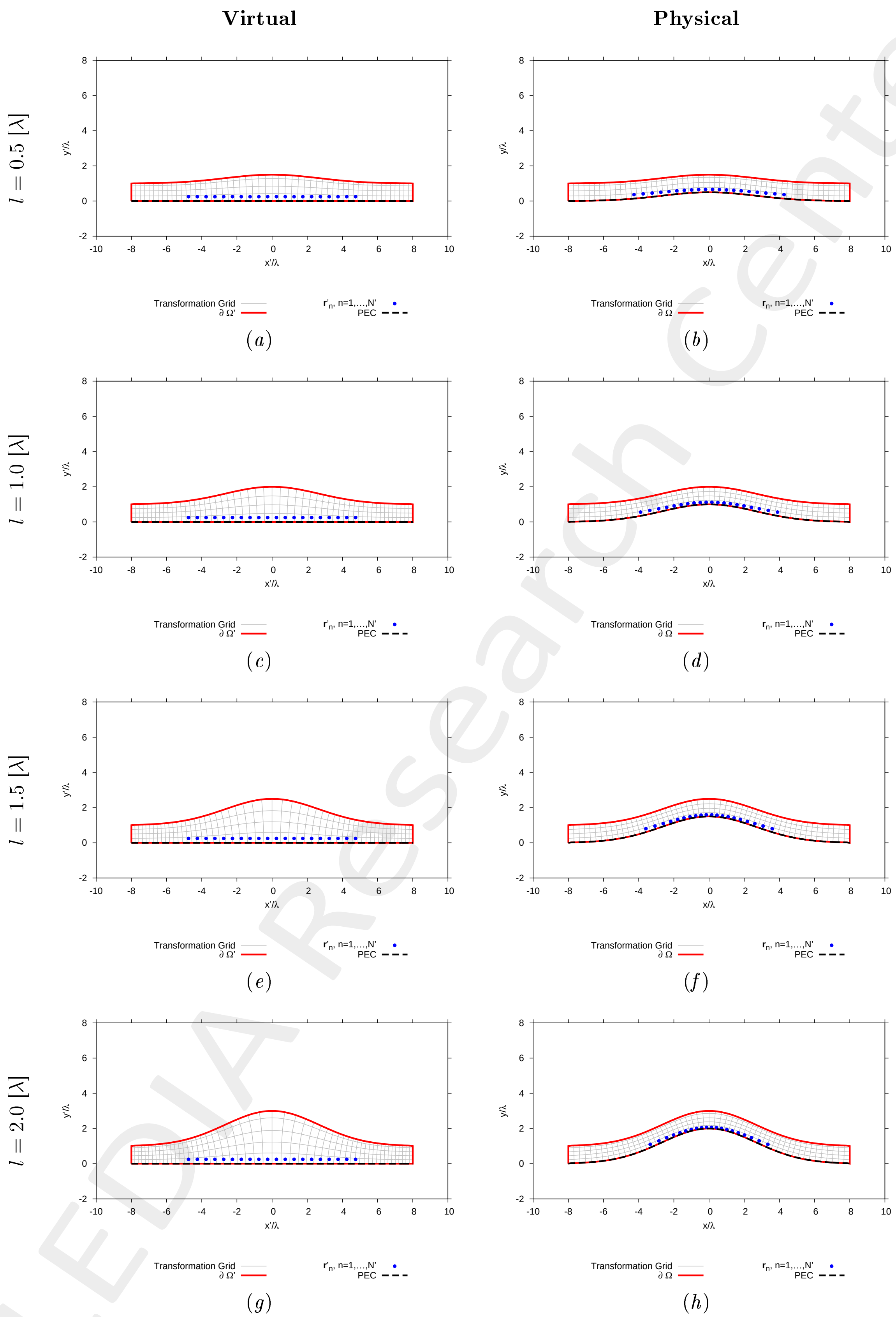

Figure 16: Lens thickness $s = 1.0$ [λ] - Transformation grids for virtual and physical geometries for different curvatures of the lens.

Lens Thickness $s = 0.5$ [λ]

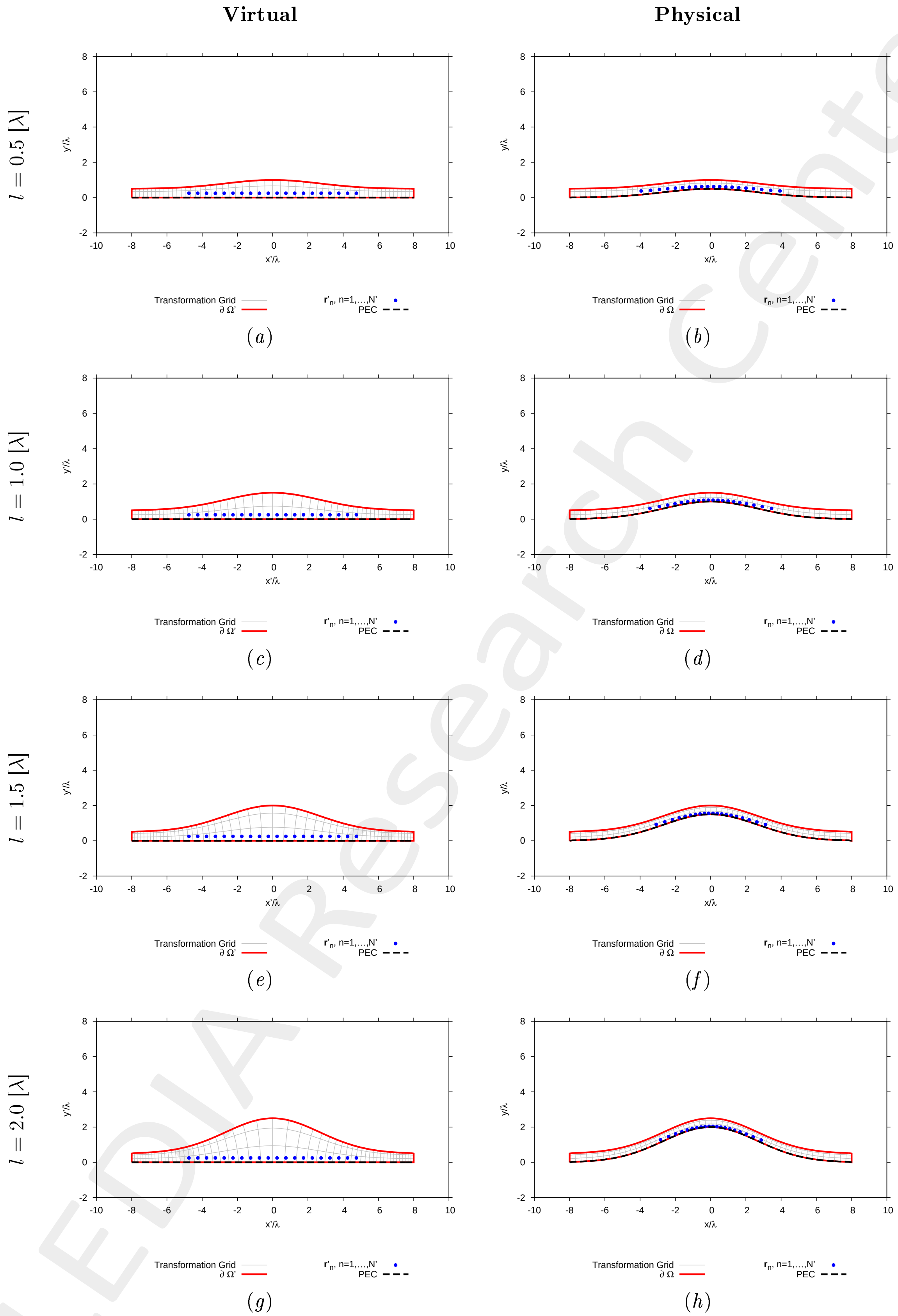

Figure 17: Lens thickness $s = 0.5$ [λ] - Transformation grids for virtual and physical geometries for different curvatures of the lens.

2.1.2 Physical Lens Parameters

Lens Curvature $l = 0.5$ [λ]				
	$s = 4.0$ [λ]	$s = 2.0$ [λ]	$s = 1.0$ [λ]	$s = 0.5$ [λ]
Anisotropic Permittivity Range	$[-0.030, 1.370]$	$[-0.040, 1.530]$	$[-0.060, 1.960]$	$[-0.110, 3.010]$
Isotropic Permittivity Range	$[0.00, 1.090]$	$[0.00, 1.120]$	$[0.00, 1.200]$	$[0.00, 1.340]$
Lens Curvature $l = 1.0$ [λ]				
	$s = 4.0$ [λ]	$s = 2.0$ [λ]	$s = 1.0$ [λ]	$s = 0.5$ [λ]
Anisotropic Permittivity Range	$[-0.070, 1.830]$	$[-0.100, 2.200]$	$[-0.170, 3.190]$	$[-0.270, 5.700]$
Isotropic Permittivity Range	$[0.00, 1.200]$	$[0.00, 1.240]$	$[0.00, 1.370]$	$[0.00, 1.600]$
Lens Curvature $l = 1.5$ [λ]				
	$s = 4.0$ [λ]	$s = 2.0$ [λ]	$s = 1.0$ [λ]	$s = 0.5$ [λ]
Anisotropic Permittivity Range	$[-0.120, 2.420]$	$[-0.200, 2.970]$	$[-0.320, 4.570]$	$[-0.470, 8.950]$
Isotropic Permittivity Range	$[0.00, 1.330]$	$[0.00, 1.360]$	$[0.00, 1.530]$	$[0.00, 1.890]$
Lens Curvature $l = 2.0$ [λ]				
	$s = 4.0$ [λ]	$s = 2.0$ [λ]	$s = 1.0$ [λ]	$s = 0.5$ [λ]
Anisotropic Permittivity Range	$[-0.190, 3.180]$	$[-0.320, 4.000]$	$[-0.480, 6.340]$	$[-0.690, 12.360]$
Isotropic Permittivity Range	$[0.00, 1.490]$	$[0.00, 1.490]$	$[0.00, 1.730]$	$[0.00, 2.180]$

Table IV: Permittivity ranges of the physical lens.

2.1.3 Far-Field Patterns (Aniso-Lens, $\phi_s = 90.0$ $[deg]$)

Lens Thickness $s = 4.0$ $[\lambda]$

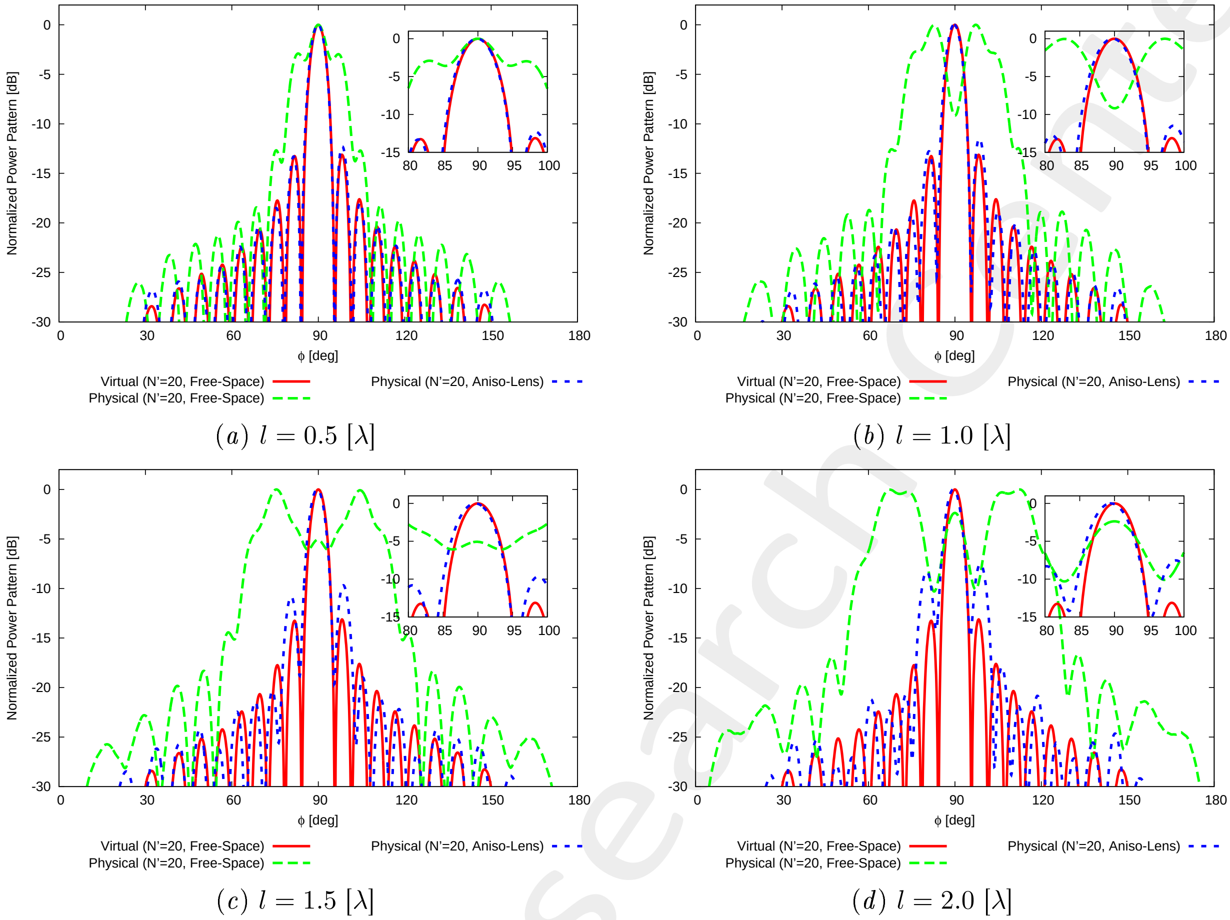

(a) $l = 0.5$ $[\lambda]$ (b) $l = 1.0$ $[\lambda]$

(c) $l = 1.5$ $[\lambda]$ (d) $l = 2.0$ $[\lambda]$

Figure 18: Lens thickness $s = 4.0$ $[\lambda]$ - Comparison between the far field patterns or different curvatures of the lens.

Lens Thickness $s = 2.0$ $[\lambda]$

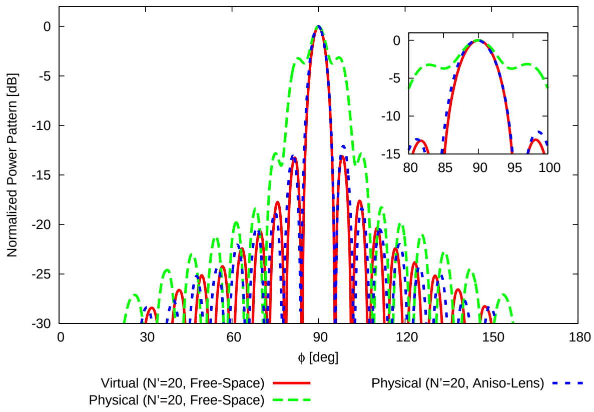

(a) $l = 0.5$ $[\lambda]$

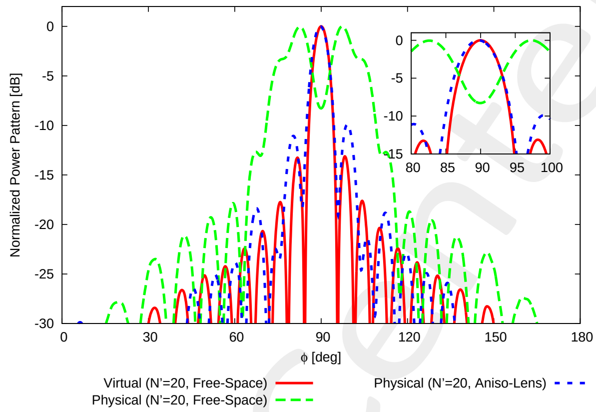

(b) $l = 1.0$ $[\lambda]$

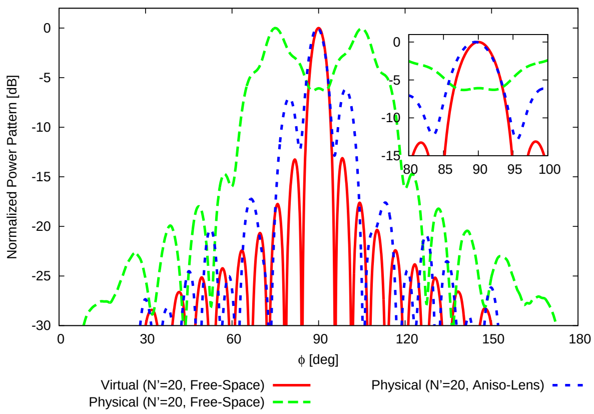

(c) $l = 1.5$ $[\lambda]$

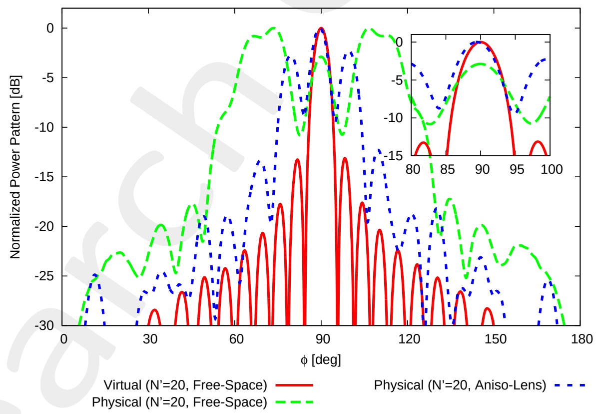

(d) $l = 2.0$ $[\lambda]$

Figure 19: Lens thickness $s = 2.0$ $[\lambda]$ - Comparison between the far field patterns or different curvatures of the lens.

Lens Thickness $s = 1.0$ $[\lambda]$

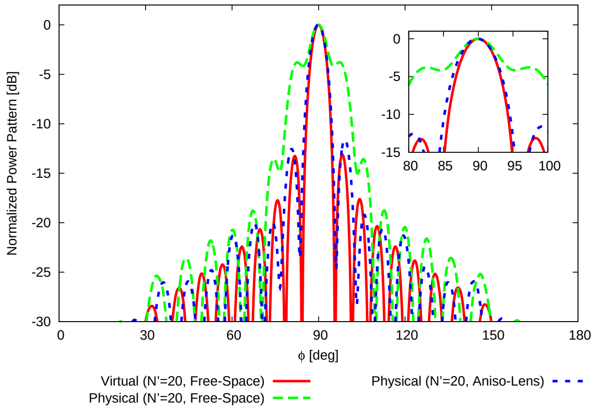

(a) $l = 0.5$ $[\lambda]$

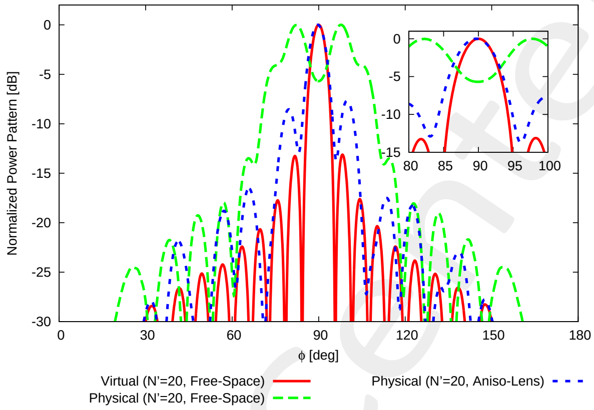

(b) $l = 1.0$ $[\lambda]$

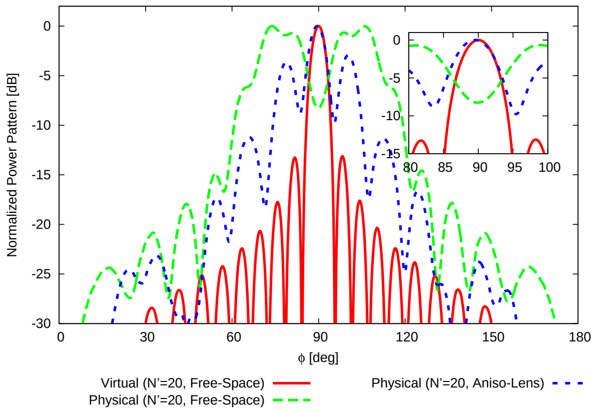

(c) $l = 1.5$ $[\lambda]$

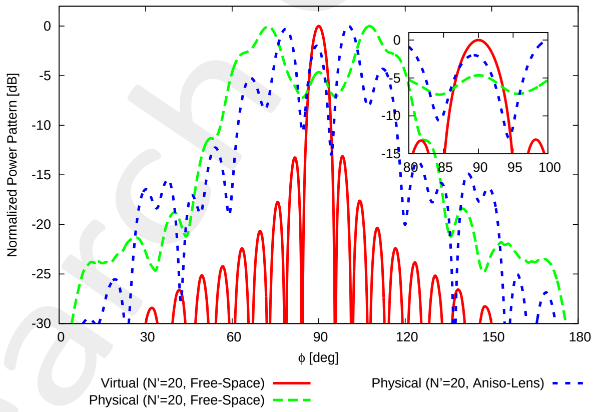

(d) $l = 2.0$ $[\lambda]$

Figure 20: Lens thickness $s = 1.0$ $[\lambda]$ - Comparison between the far field patterns or different curvatures of the lens.

Lens Thickness $s = 0.5$ [λ]

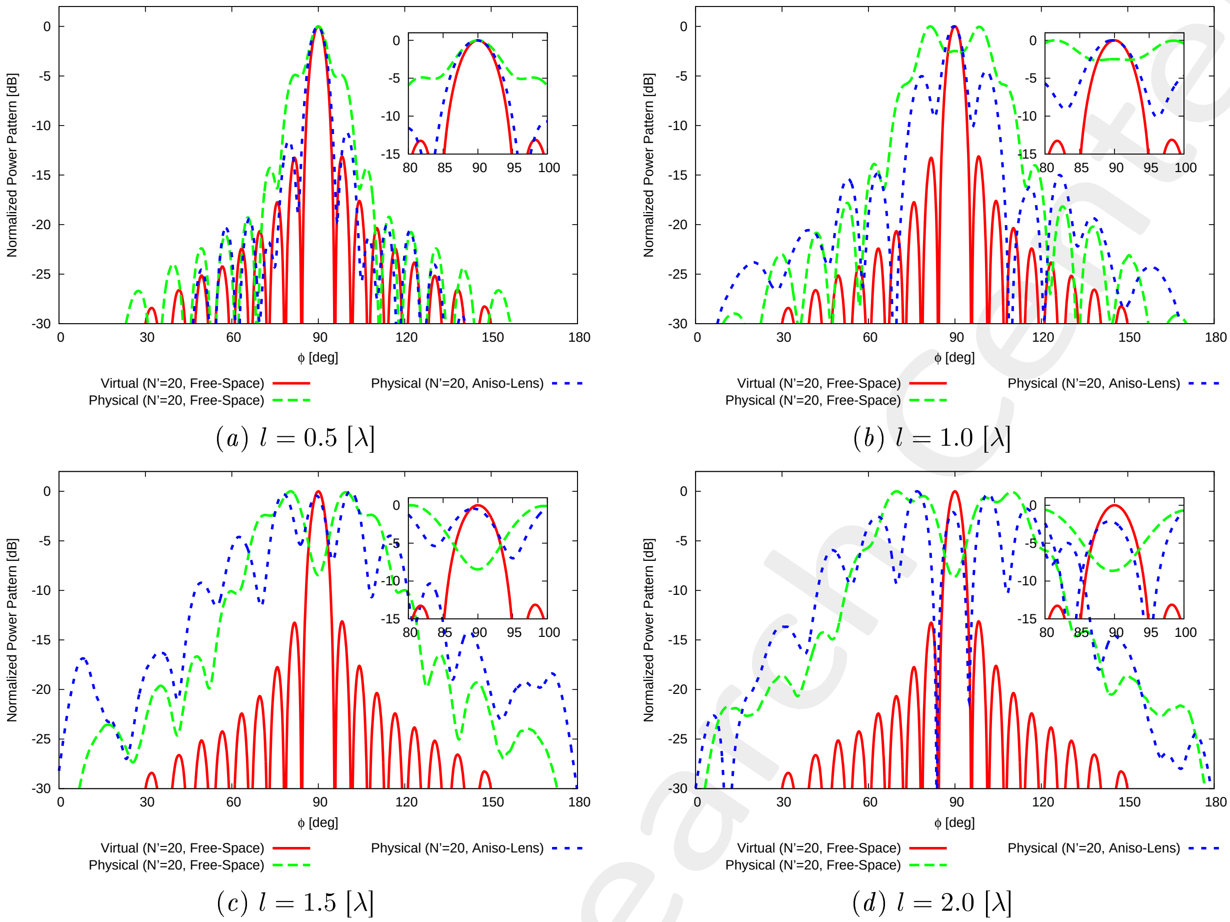

(a) $l = 0.5$ [λ] (b) $l = 1.0$ [λ]

(c) $l = 1.5$ [λ] (d) $l = 2.0$ [λ]

Figure 21: Lens thickness $s = 0.5$ [λ] - Comparison between the far field patterns or different curvatures of the lens.

Observations

- Increasing the curvature ($\uparrow l$) leads to a worsening of the performances;
- Decreasing the lens thickness ($\downarrow s$) leads to a worsening of the performances;
- The thinner the lens, the fastest the degradation w.r.t. the curvature.

2.2 Final Resume

2.2.1 Pattern Performances vs. Lens Curvature (l)

Before SI ($\phi_s = 90$ [deg], $f = 600$[MHz])

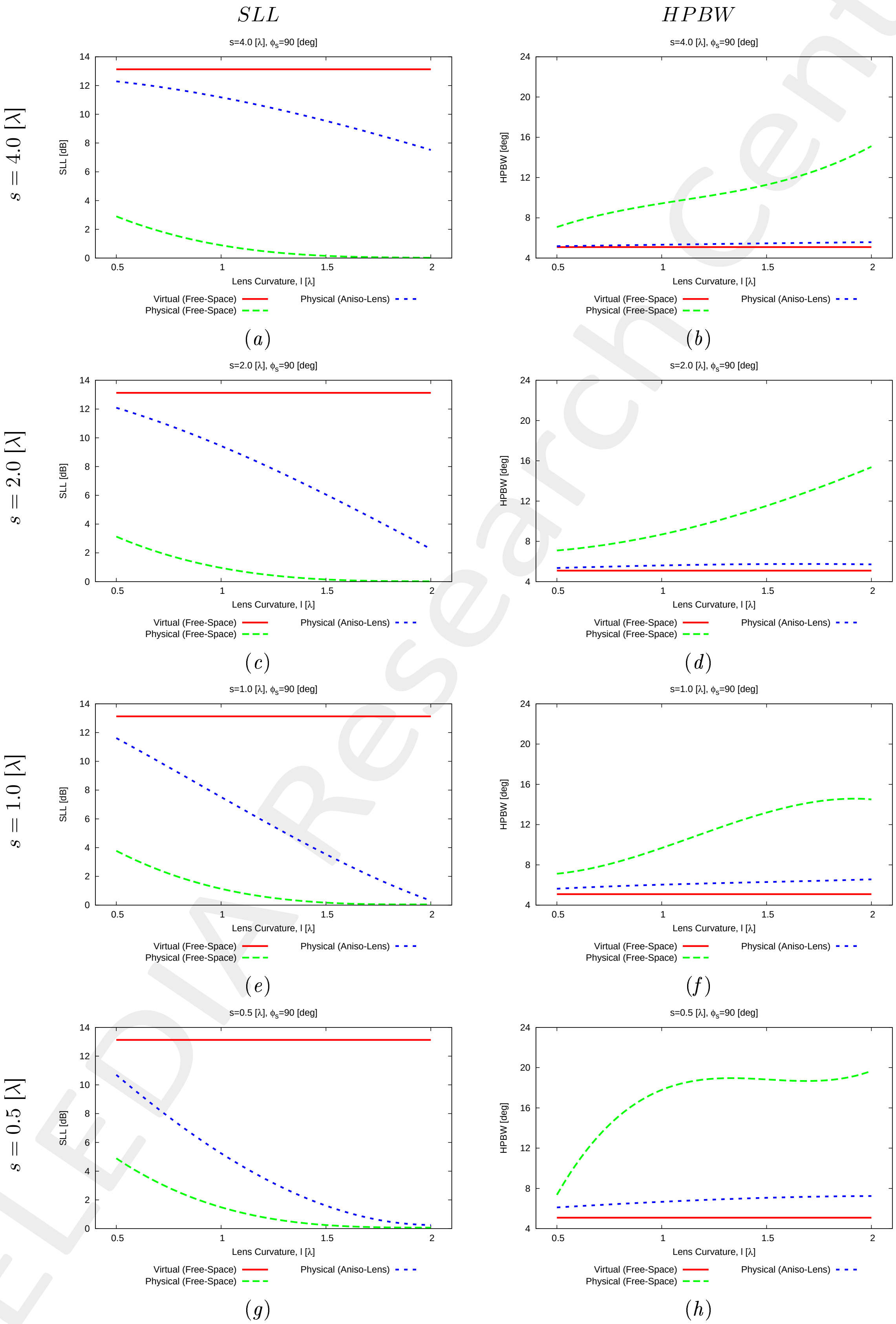

Figure 22: $\phi_s = 90$ [deg], $f = 600$[MHz] - SLL and $HPBW$ vs. the lens curvature (l).

2.2.2 Pattern Performances vs. Lens Thickness (s)

Before SI ($\phi_s = 90$ [deg], $f = 600$[MHz])

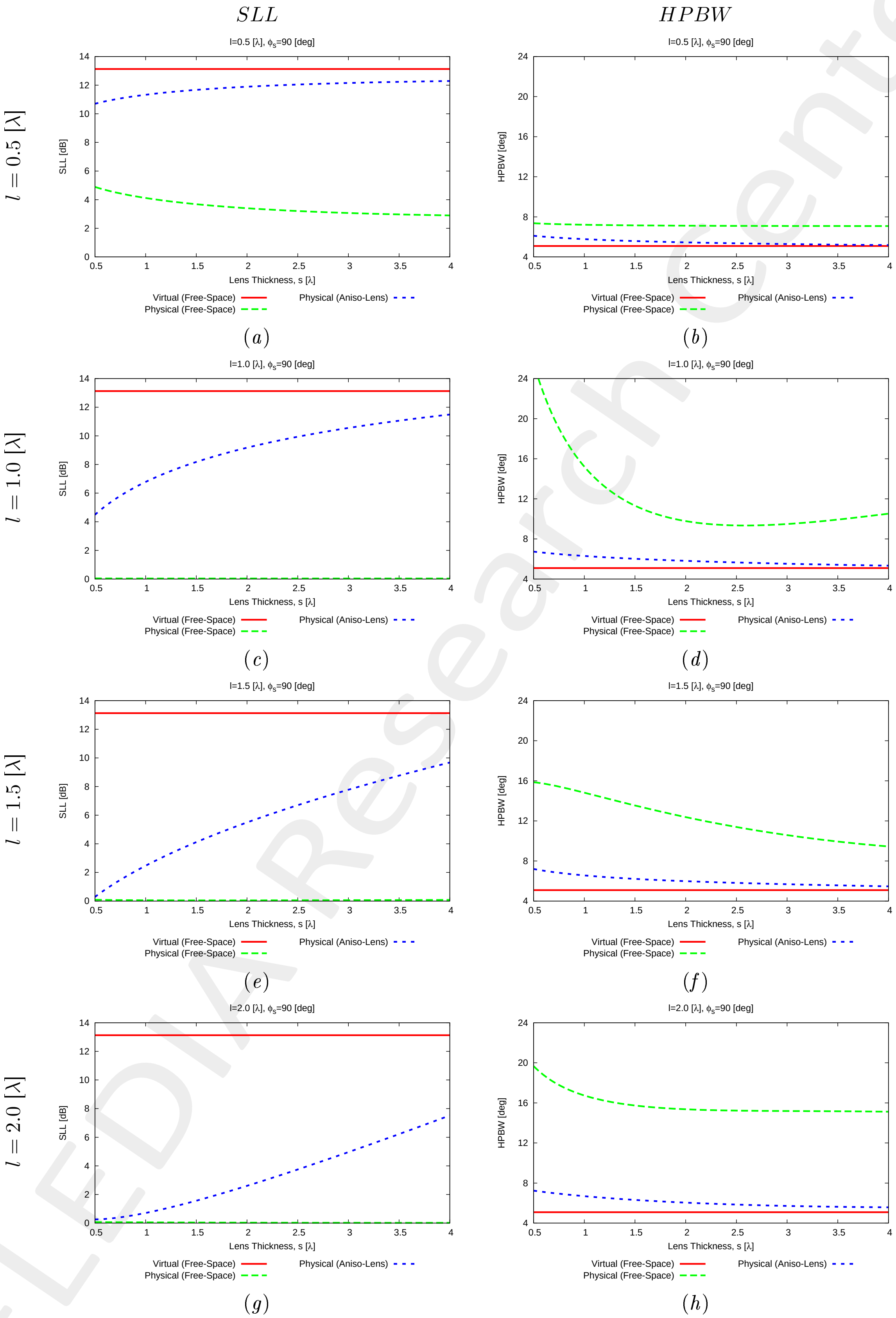

Figure 23: $\phi_s = 90$ [deg], $f = 600$[MHz] - SLL and $HPBW$ vs. the lens thickness (s).

2.2.3 Pattern Performances vs. Lens Curvature (l) and vs. Lens Thickness (s)

Before SI ($\phi_s = 90$ [deg], $f = 600$[MHz] - Physical Array (Aniso-Lens))

Characteristics of the virtual array ($N' = 20$, Free-Space)

- $SLL = 13.13$ [dB];
- $FNBW = 11.44$ [deg];
- $HPBW = 5.09$ [deg];

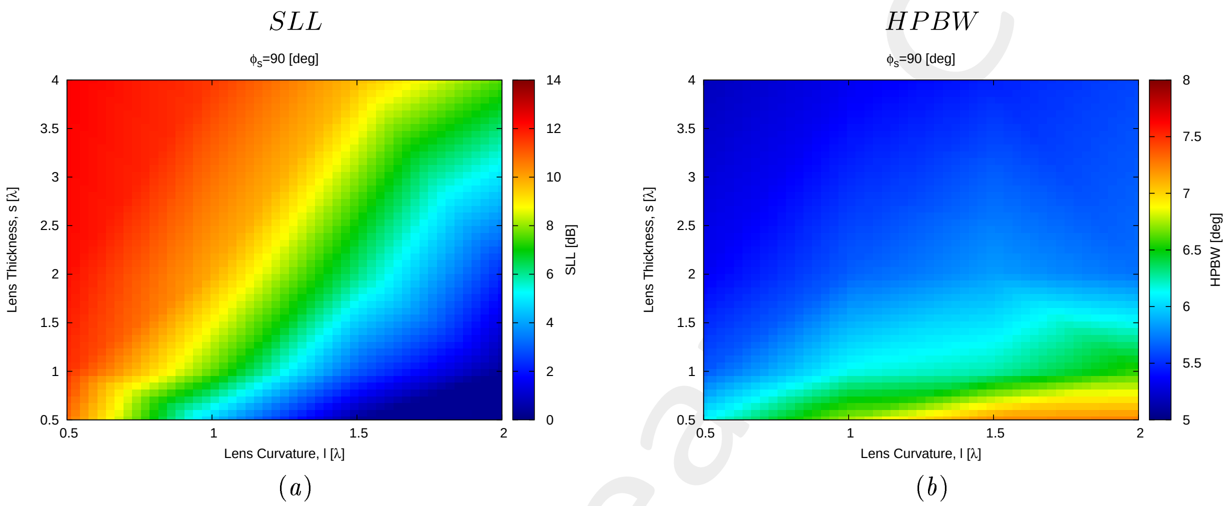

Figure 24: $\phi_s = 90$ [deg], $f = 600$[MHz] - SLL and $HPBW$ vs. the lens thickness (s) and the lens curvature (l).

3 "Elliptic Arc" Geometry - $N' = 20$

3.1 Validation vs. Lens Curvature (l) and Lens Thickness (s)

Input Parameters

- **Virtual & Physical Geometries**

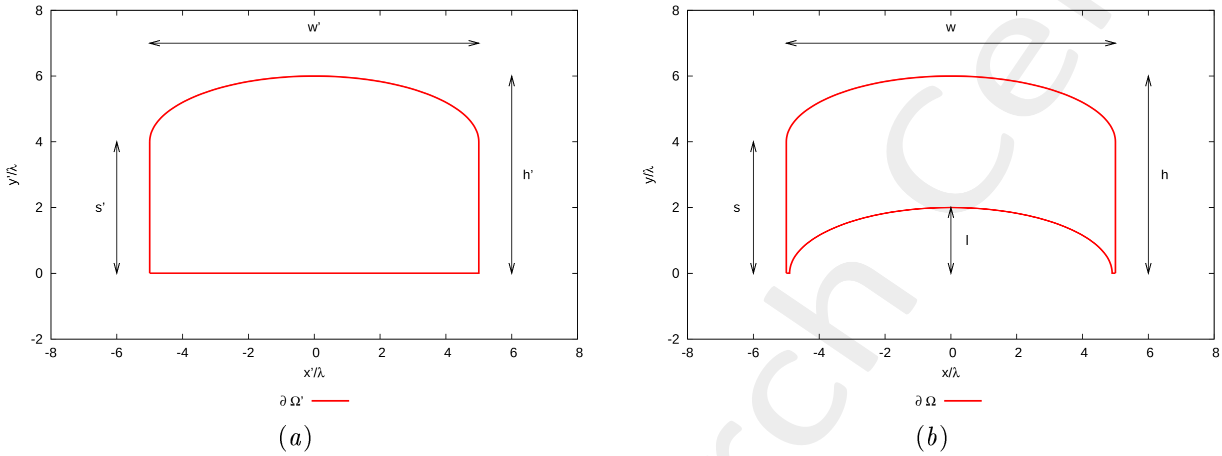

Figure 25: Transformation regions and geometric parameters of interest.

  - The two-half ellipses (lower and higher) have semi-axis along x equal to $w/2$ ($= w'/2$) and semi-axis along y equal to l.

Lens Thickness: $s = 4.0$ $[\lambda]$						
Virtual			**Physical**			
w' $[\lambda]$	h' $[\lambda]$	s' $[\lambda]$	w $[\lambda]$	h $[\lambda]$	s $[\lambda]$	l $[\lambda]$ (Curvature)
16.0	4.5	4.0	16.0	4.5	4.0	**0.5**
16.0	5.0	4.0	16.0	5.0	4.0	**1.0**
16.0	5.5	4.0	16.0	5.5	4.0	**1.5**
16.0	6.0	4.0	16.0	6.0	4.0	**2.0**

Lens Thickness: $s = 2.0$ $[\lambda]$						
Virtual			**Physical**			
w' $[\lambda]$	h' $[\lambda]$	s' $[\lambda]$	w $[\lambda]$	h $[\lambda]$	s $[\lambda]$	l $[\lambda]$ (Curvature)
16.0	2.5	2.0	16.0	2.5	2.0	**0.5**
16.0	3.0	2.0	16.0	3.0	2.0	**1.0**
16.0	3.5	2.0	16.0	3.5	2.0	**1.5**
16.0	4.0	2.0	16.0	4.0	2.0	**2.0**

Lens Thickness: $s = 1.0$ $[\lambda]$						
Virtual			**Physical**			
w' $[\lambda]$	h' $[\lambda]$	s' $[\lambda]$	w $[\lambda]$	h $[\lambda]$	s $[\lambda]$	l $[\lambda]$ (Curvature)
16.0	1.5	1.0	16.0	1.5	1.0	**0.5**
16.0	2.0	1.0	16.0	2.0	1.0	**1.0**
16.0	2.5	1.0	16.0	2.5	1.0	**1.5**
16.0	3.0	1.0	16.0	3.0	1.0	**2.0**

Lens Thickness: $s = 0.5$ $[\lambda]$						
Virtual			**Physical**			
w' $[\lambda]$	h' $[\lambda]$	s' $[\lambda]$	w $[\lambda]$	h $[\lambda]$	s $[\lambda]$	l $[\lambda]$ (Curvature)
16.0	1.0	0.5	16.0	1.0	0.5	**0.5**
16.0	1.5	0.5	16.0	1.5	0.5	**1.0**
16.0	2.0	0.5	16.0	2.0	0.5	**1.5**
16.0	2.5	0.5	16.0	2.5	0.5	**2.0**

Table V: Geometric descriptors for virtual and physical geometries. Note that $w' = w$, $h' = h$, $s' = s$, and $h = s + l$.

- **Virtual Array**
  - Number of elements, spacing, aperture: $N' = 20$, $d' = \frac{\lambda}{2}$, $L' = 9.5$ $[\lambda]$;
  - Distance from PEC ground plane (placed at $y' = 0.0$): $\delta' = \frac{\lambda}{4}$;
  - Operating frequency: $f = 600$ $[MHz]$;
  - Steering angle: $\phi_s = 90.0$ $[deg]$;
  - Excitations: $I_n = 1.0$, $\varphi_n = \frac{-2\pi}{\lambda} x_n sin\left(\phi_s + 90\right)$; $n = 1, ..., N'$;
- **QCTO**
  - Discretization cell dimension: 0.15 $[\lambda]$ (0.01 $[\lambda]$ for source mapping);

3.1.1 Results of the Transformation

Lens Thickness $s = 4.0$ [λ]

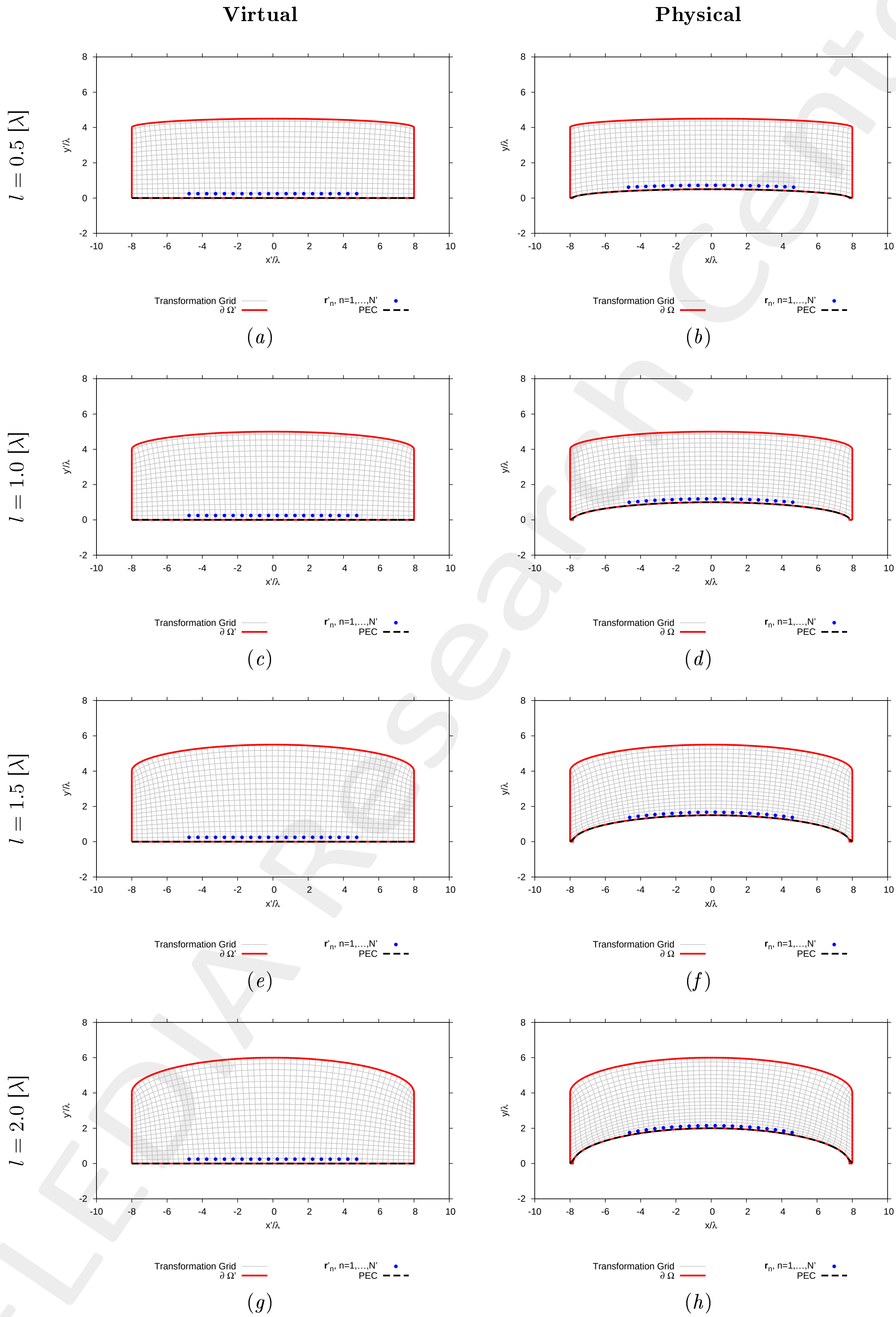

Figure 26: Lens thickness $s = 4.0$ [λ] - Transformation grids for virtual and physical geometries for different curvatures of the lens.

Lens Thickness $s = 2.0$ [λ]

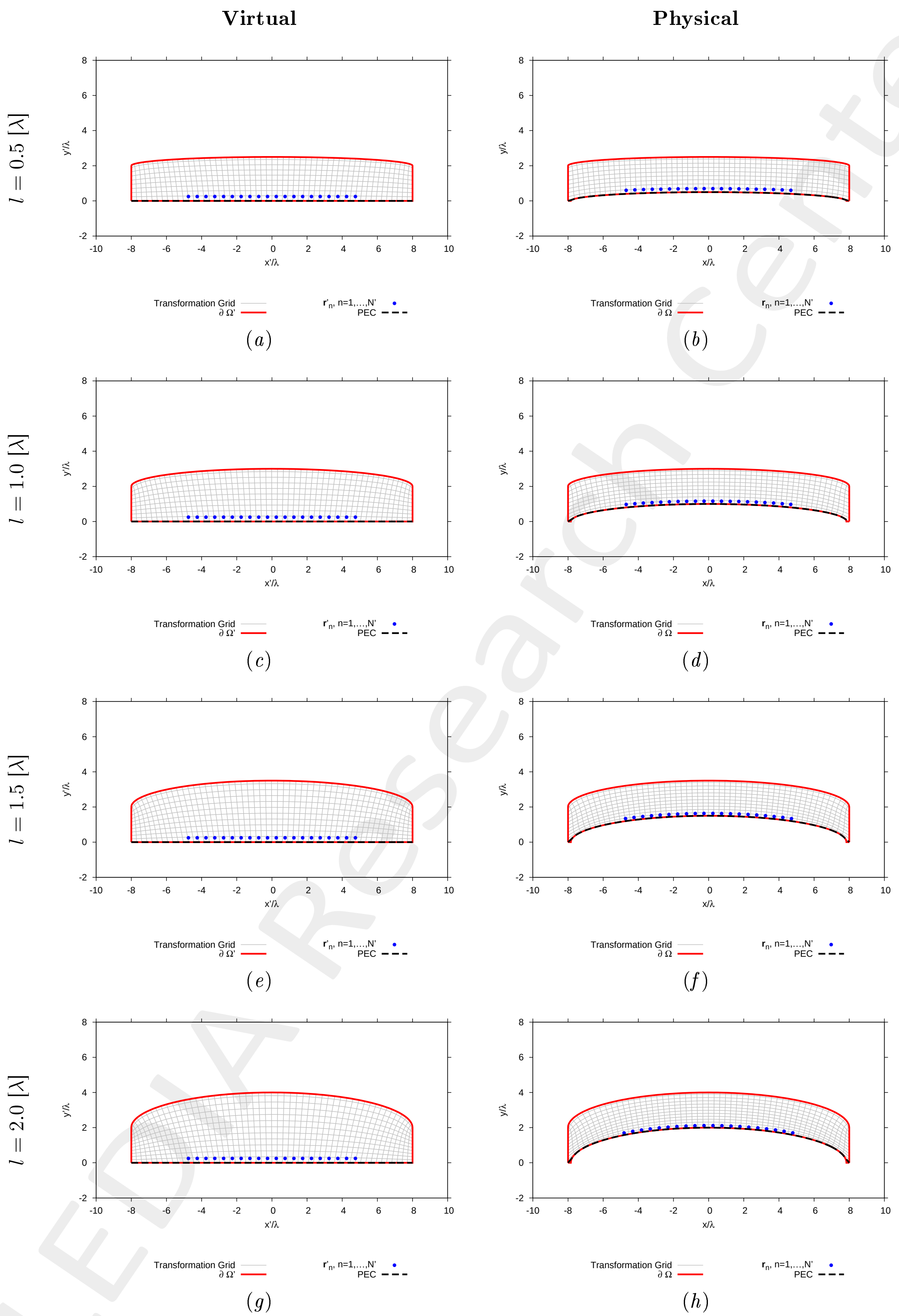

Figure 27: Lens thickness $s = 2.0$ [λ] - Transformation grids for virtual and physical geometries for different curvatures of the lens.

Lens Thickness $s = 1.0$ $[\lambda]$

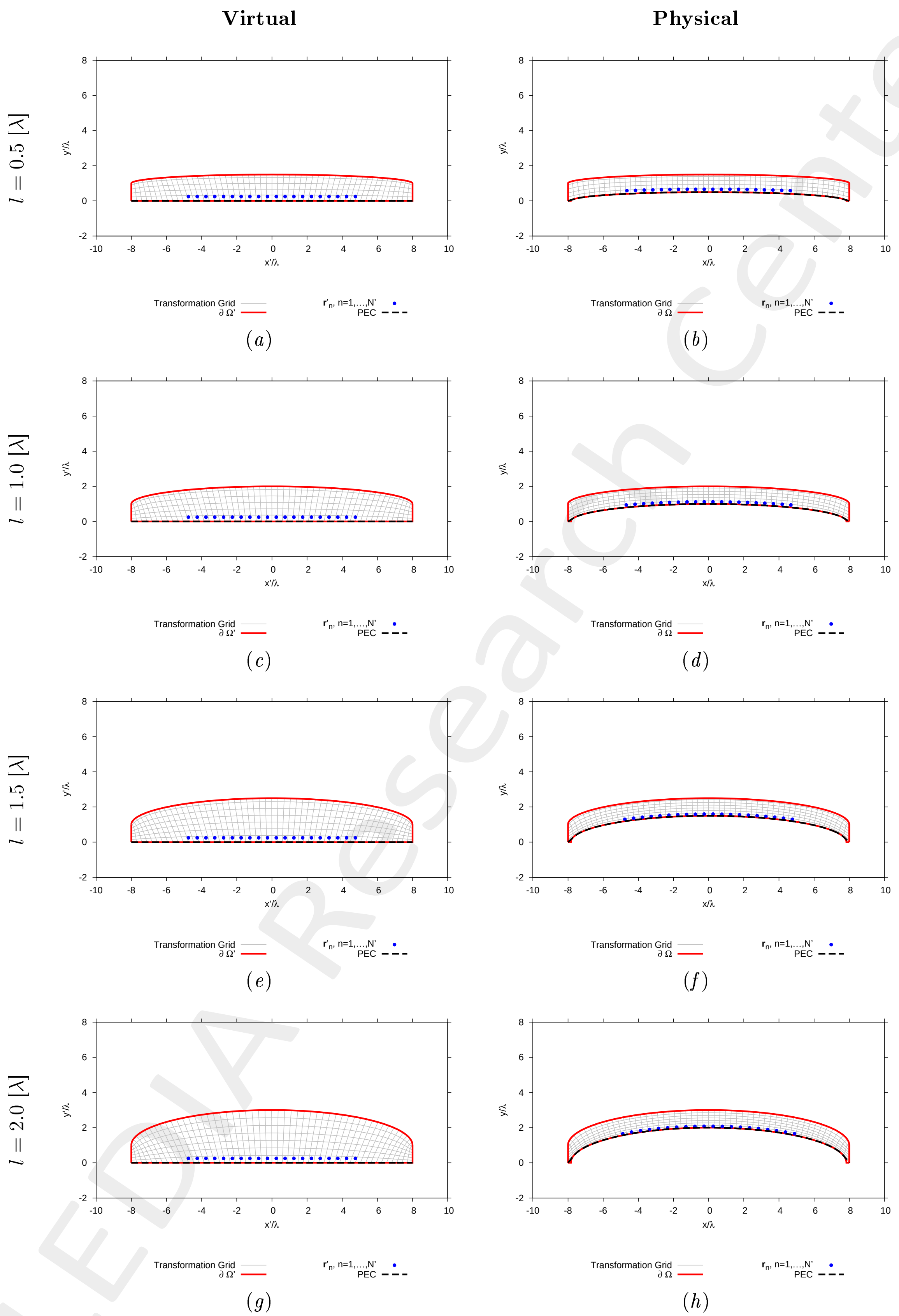

Figure 28: Lens thickness $s = 1.0$ $[\lambda]$ - Transformation grids for virtual and physical geometries for different curvatures of the lens.

Lens Thickness $s = 0.5$ [λ]

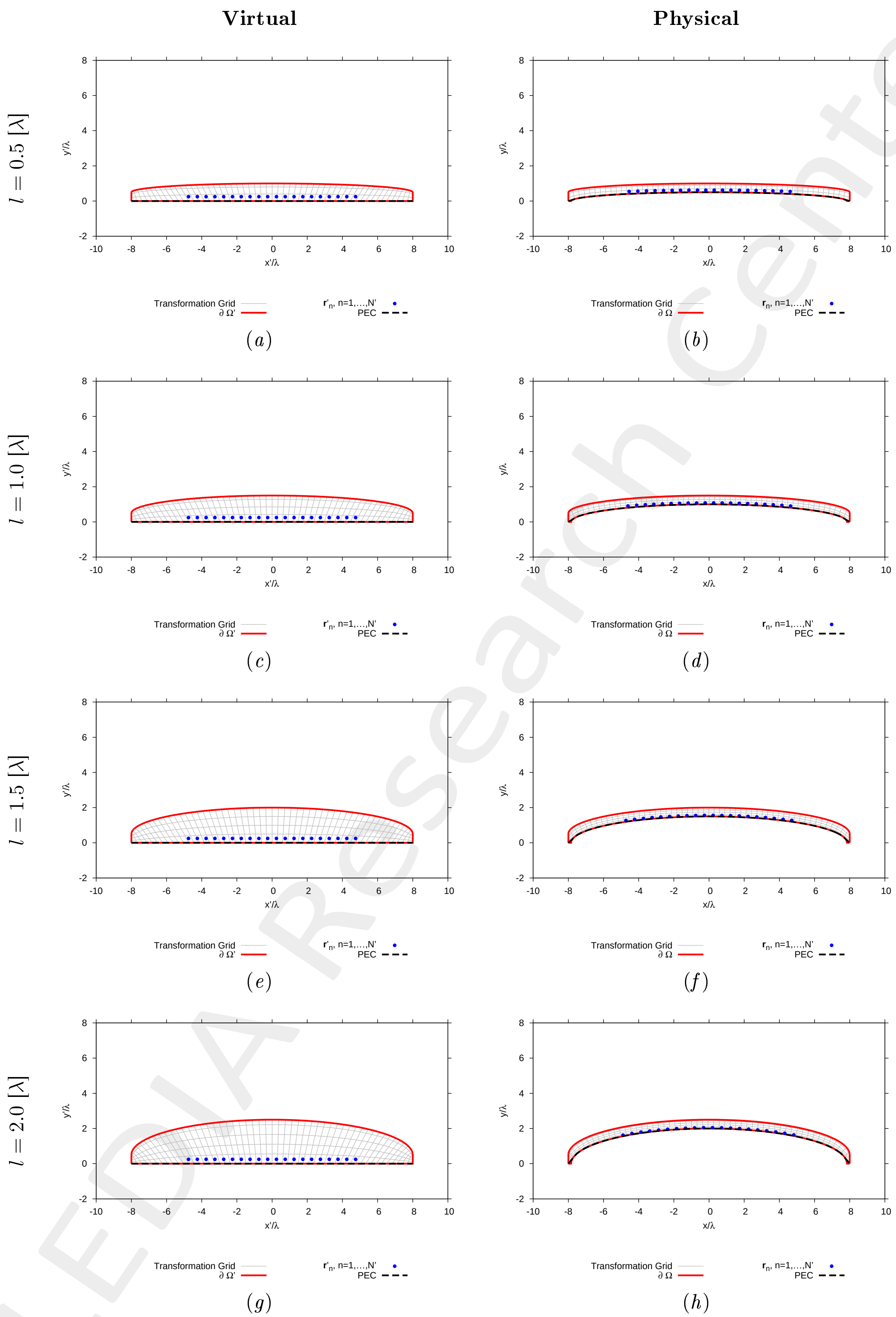

Figure 29: Lens thickness $s = 0.5$ [λ] - Transformation grids for virtual and physical geometries for different curvatures of the lens.

3.1.2 Physical Lens Parameters

Lens Curvature $l = 0.5$ [λ]				
	$s = 4.0$ [λ]	$s = 2.0$ [λ]	$s = 1.0$ [λ]	$s = 0.5$ [λ]
Anisotropic Permittivity Range	$[-0.290, 1.690]$	$[-0.310, 1.800]$	$[-0.350, 1.800]$	$[-0.720, 2.310]$
Isotropic Permittivity Range	$[0.00, 1.400]$	$[0.00, 1.440]$	$[0.00, 1.480]$	$[0.00, 1.910]$
Lens Curvature $l = 1.0$ [λ]				
	$s = 4.0$ [λ]	$s = 2.0$ [λ]	$s = 1.0$ [λ]	$s = 0.5$ [λ]
Anisotropic Permittivity Range	$[-1.300, 2.520]$	$[-1.390, 2.740]$	$[-1.290, 2.650]$	$[-1.060, 3.440]$
Isotropic Permittivity Range	$[0.00, 1.600]$	$[0.00, 1.610]$	$[0.00, 1.920]$	$[0.00, 2.710]$
Lens Curvature $l = 1.5$ [λ]				
	$s = 4.0$ [λ]	$s = 2.0$ [λ]	$s = 1.0$ [λ]	$s = 0.5$ [λ]
Anisotropic Permittivity Range	$[-3.060, 3.620]$	$[-3.230, 3.870]$	$[-2.860, 3.610]$	$[-1.920, 4.560]$
Isotropic Permittivity Range	$[0.00, 1.650]$	$[0.00, 1.640]$	$[0.00, 2.550]$	$[0.00, 4.340]$
Lens Curvature $l = 2.0$ [λ]				
	$s = 4.0$ [λ]	$s = 2.0$ [λ]	$s = 1.0$ [λ]	$s = 0.5$ [λ]
Anisotropic Permittivity Range	$[-6.100, 13.010]$	$[-6.260, 21.810]$	$[-4.620, 7.510]$	$[-3.410, 5.930]$
Isotropic Permittivity Range	$[0.00, 1.630]$	$[0.00, 1.670]$	$[0.00, 2.830]$	$[0.00, 4.110]$

Table VI: Permittivity ranges of the physical lens.

3.1.3 Far-Field Patterns (Aniso-Lens, $\phi_s = 90.0$ $[deg]$)

Lens Thickness $s = 4.0$ $[\lambda]$

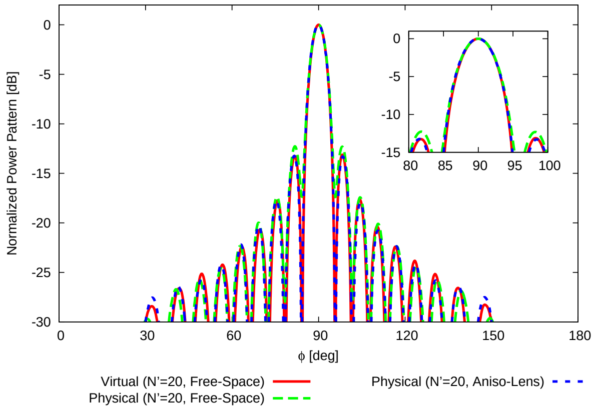

(a) $l = 0.5$ $[\lambda]$

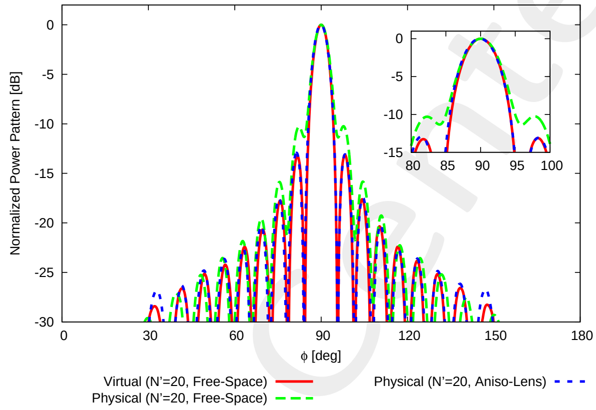

(b) $l = 1.0$ $[\lambda]$

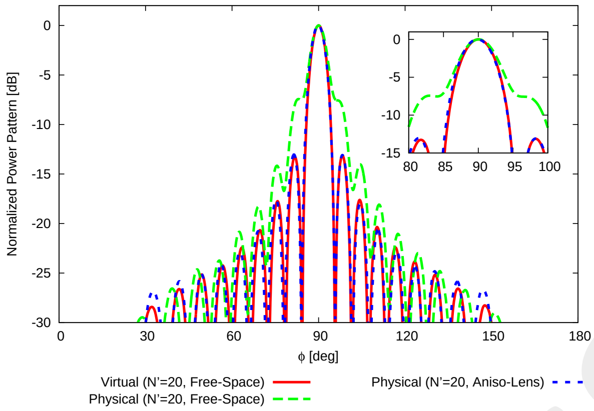

(c) $l = 1.5$ $[\lambda]$

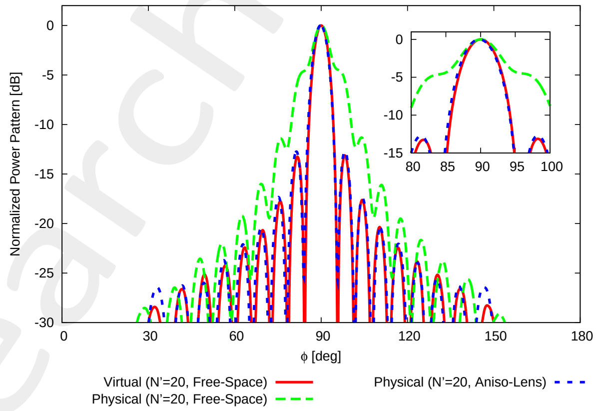

(d) $l = 2.0$ $[\lambda]$

Figure 30: Lens thickness $s = 4.0$ $[\lambda]$ - Comparison between the far field patterns or different curvatures of the lens.

Lens Thickness $s = 2.0$ $[\lambda]$

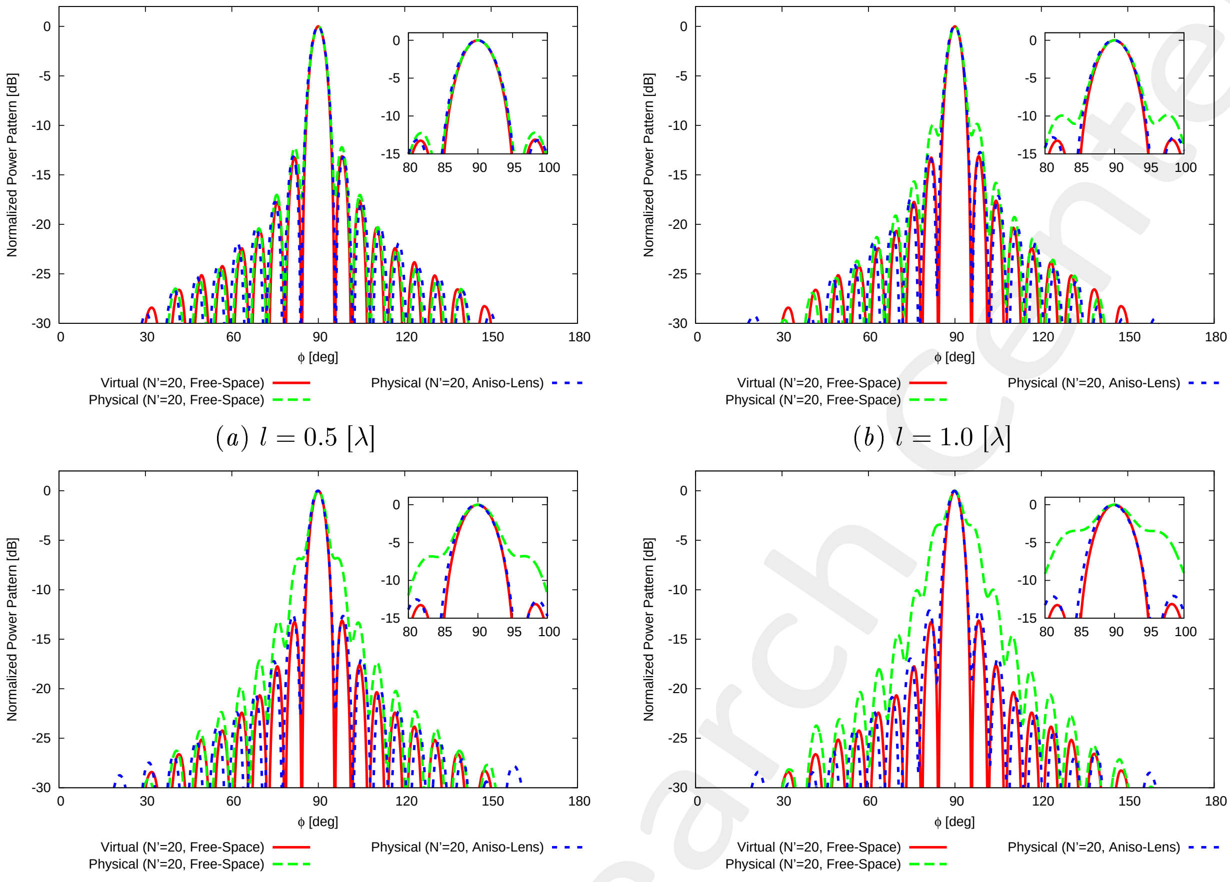

(a) $l = 0.5$ $[\lambda]$ (b) $l = 1.0$ $[\lambda]$

(c) $l = 1.5$ $[\lambda]$ (d) $l = 2.0$ $[\lambda]$

Figure 31: Lens thickness $s = 2.0$ $[\lambda]$ - Comparison between the far field patterns or different curvatures of the lens.

Lens Thickness $s = 1.0$ [λ]

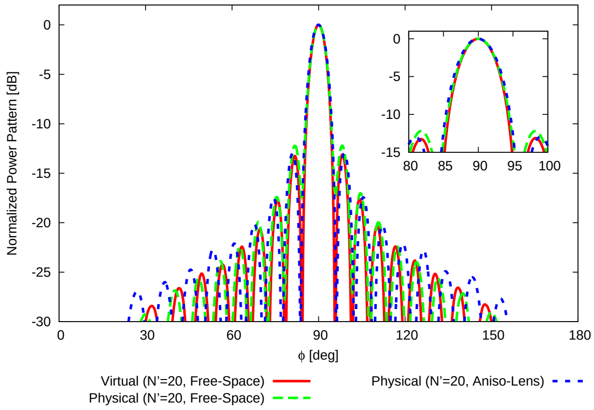

(a) $l = 0.5$ [λ]

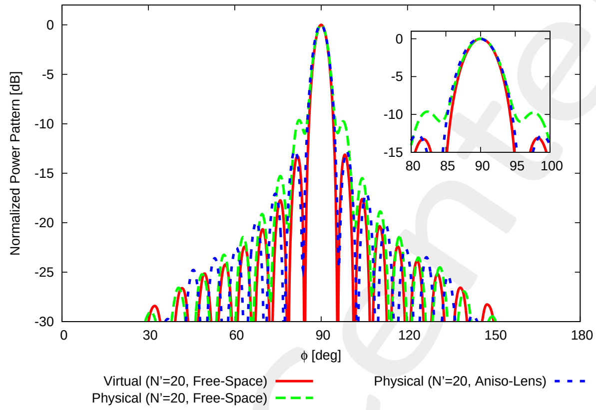

(b) $l = 1.0$ [λ]

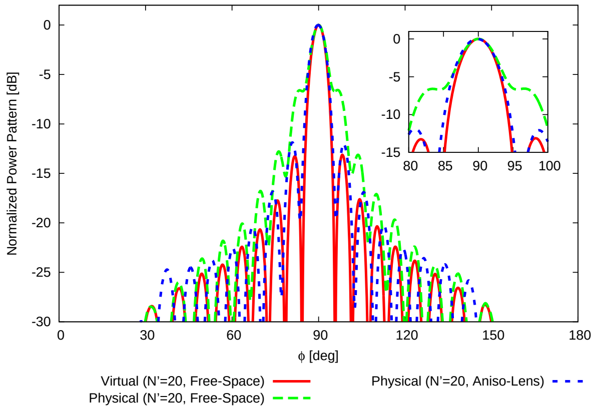

(c) $l = 1.5$ [λ]

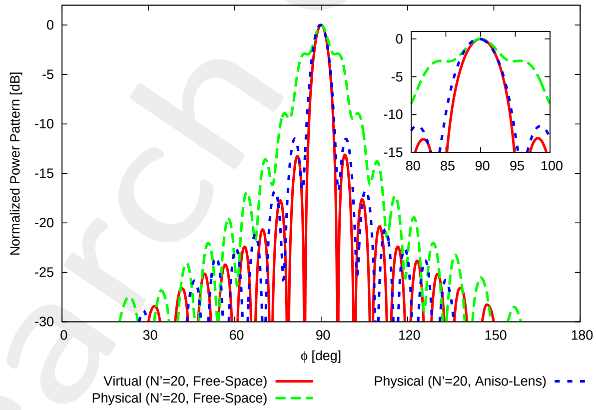

(d) $l = 2.0$ [λ]

Figure 32: Lens thickness $s = 1.0$ [λ] - Comparison between the far field patterns or different curvatures of the lens.

Lens Thickness $s = 0.5$ $[\lambda]$

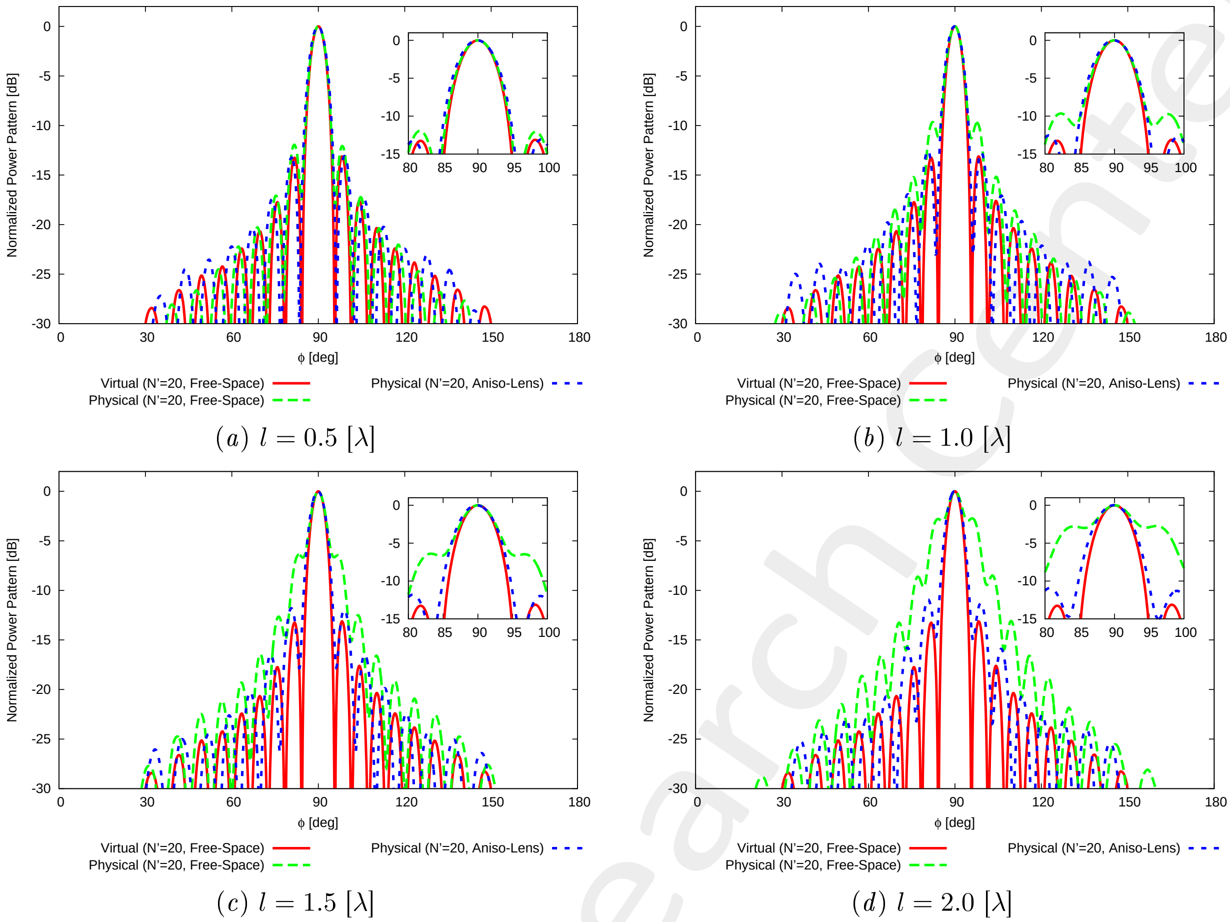

Figure 33: Lens thickness $s = 0.5$ $[\lambda]$ - Comparison between the far field patterns or different curvatures of the lens.

Observations

- Increasing the curvature ($\uparrow l$) leads to a worsening of the performances;
- Decreasing the lens thickness ($\downarrow s$) leads to a worsening of the performances;
- The thinner the lens, the fastest the degradation w.r.t. the curvature.

3.2 Final Resume

3.2.1 Pattern Performances vs. Lens Curvature (l)

Before SI ($\phi_s = 90$ [deg], $f = 600$[MHz])

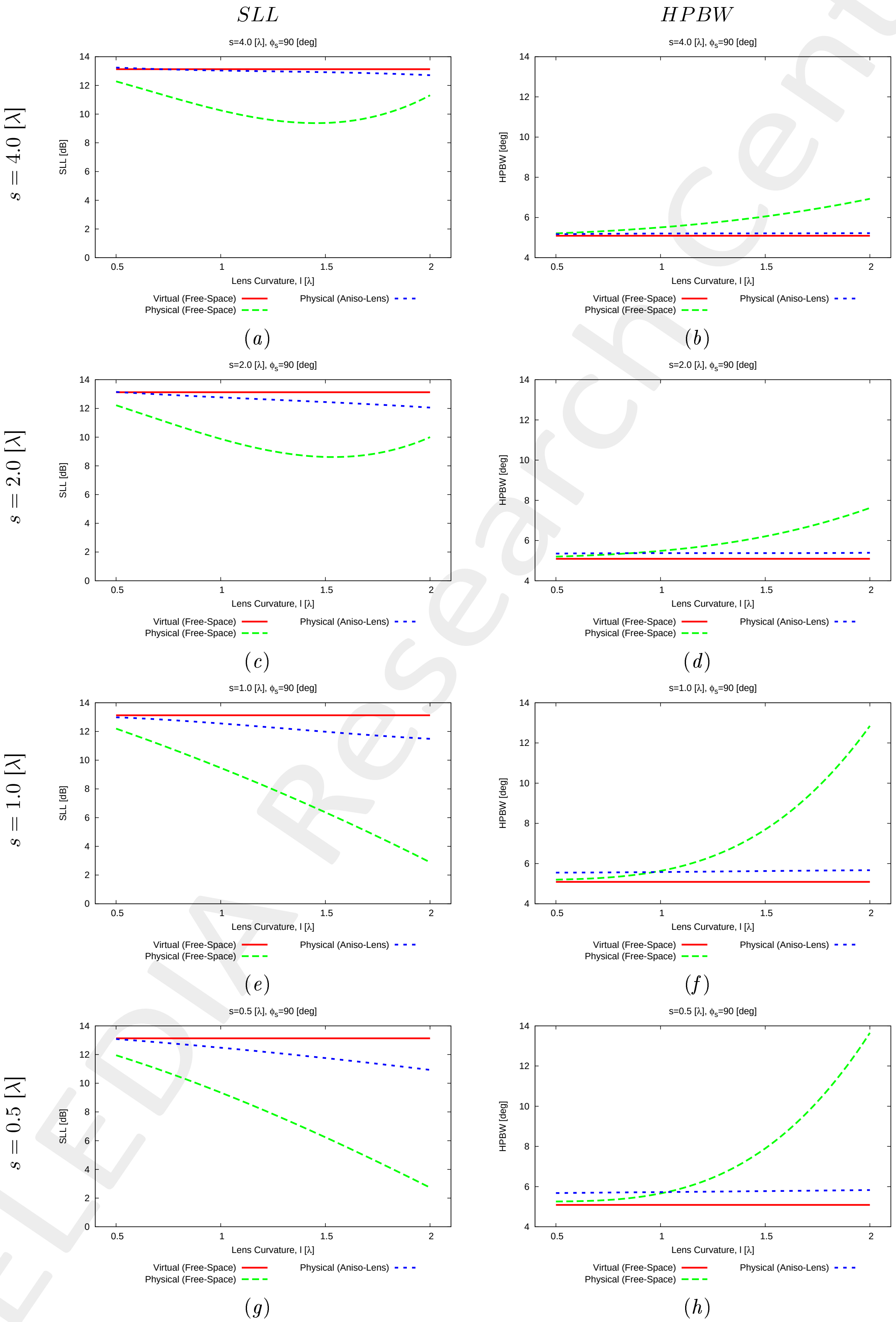

Figure 34: $\phi_s = 90$ [deg], $f = 600$[MHz] - SLL and $HPBW$ vs. the lens curvature (l).

3.2.2 Pattern Performances vs. Lens Thickness (s)

Before SI ($\phi_s = 90$ [deg], $f = 600$[MHz])

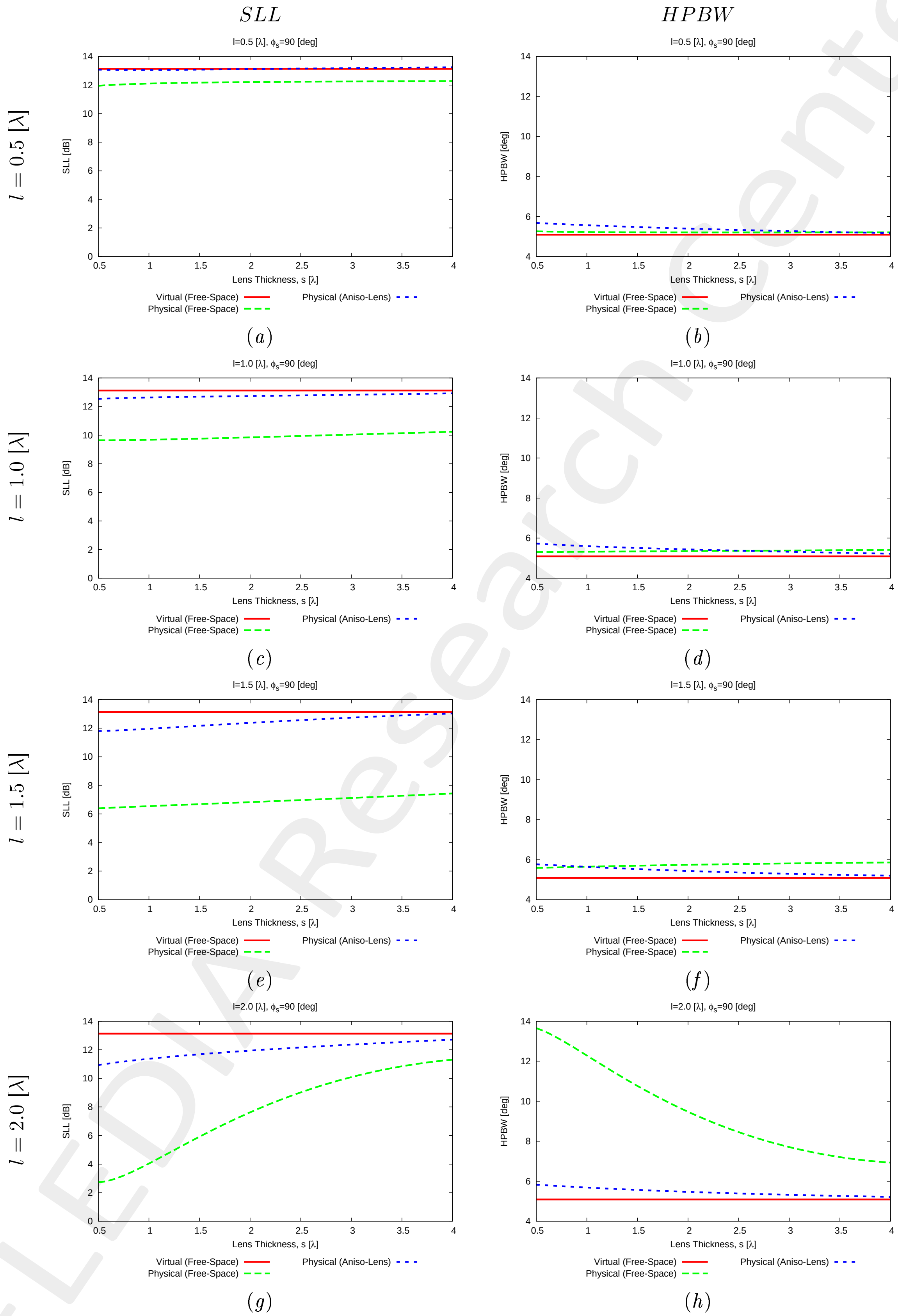

Figure 35: $\phi_s = 90$ [deg], $f = 600$[MHz] - SLL and $HPBW$ vs. the lens thickness (s).

3.2.3 Pattern Performances vs. Lens Curvature (l) and vs. Lens Thickness (s)

Before SI ($\phi_s = 90$ [deg], $f = 600$[MHz] - Physical Array (Aniso-Lens))

Characteristics of the virtual array ($N' = 20$, Free-Space)

- $SLL = 13.13$ [dB];
- $FNBW = 11.44$ [deg];
- $HPBW = 5.09$ [deg];

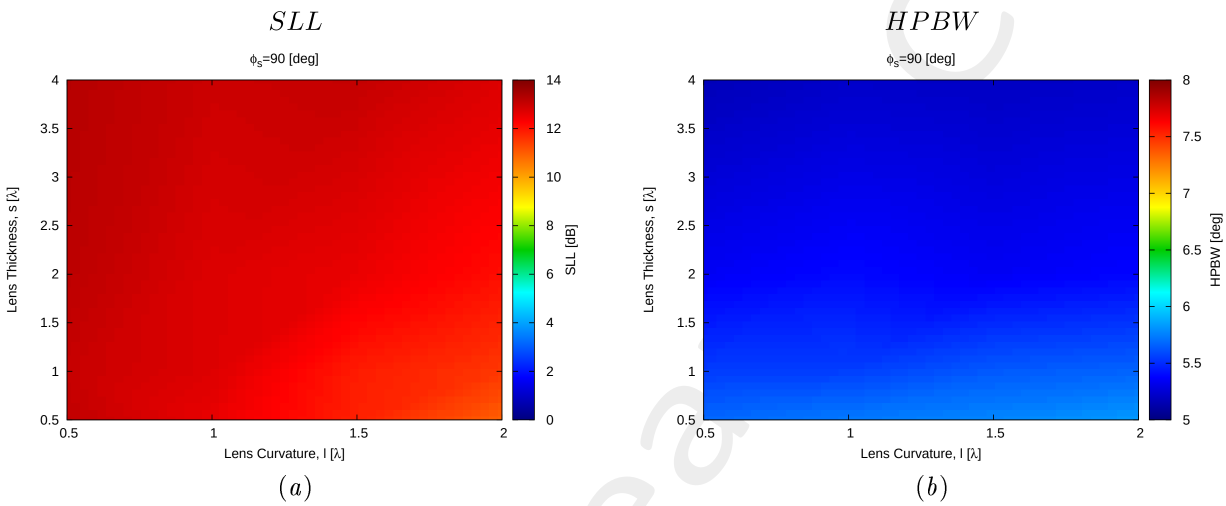

Figure 36: $\phi_s = 90$ [deg], $f = 600$[MHz] - SLL and $HPBW$ vs. the lens thickness (s) and the lens curvature (l).

References

[1] G. Oliveri, G. Gottardi, F. Robol, A. Polo, L. Poli, M. Salucci, M. Chuan, C. Massagrande, P. Vinetti, M. Mattivi, R. Lombardi, and A. Massa, "Co-design of unconventional array architectures and antenna elements for 5G base station," *IEEE Trans. Antennas Propag.*, vol. 65, no. 12, pp. 6752-6767, Dec. 2017.

[2] P. Rocca, G. Oliveri, R. J. Mailloux, and A. Massa, "Unconventional phased array architectures and design methodologies - A review," *Proc. IEEE*, vol. 104, no. 3, pp. 544-560, Mar. 2016.

[3] G. Oliveri, M. Salucci, N. Anselmi and A. Massa, "Multiscale System-by-Design synthesis of printed WAIMs for waveguide array enhancement," *IEEE J. Multiscale Multiphysics Computat. Techn.*, vol. 2, pp. 84-96, 2017.

[4] A. Massa and G. Oliveri, "Metamaterial-by-Design: Theory, methods, and applications to communications and sensing - Editorial," *EPJ Applied Metamaterials*, vol. 3, no. E1, pp. 1-3, 2016.

[5] L. Poli, G. Oliveri, P. Rocca, M. Salucci, and A. Massa, "Long-Distance WPT Unconventional Arrays Synthesis," *J. Electromagnet. Waves Appl.*, vol. 31, no. 14, pp. 1399-1420, Jul. 2017.

[6] G. Oliveri, F. Viani, N. Anselmi, and A. Massa, "Synthesis of multi-layer WAIM coatings for planar phased arrays within the system-by-design framework," *IEEE Trans. Antennas Propag.*, vol. 63, no. 6, pp. 2482-2496, Jun. 2015.

[7] G. Oliveri, L. Tenuti, E. Bekele, M. Carlin, and A. Massa, "An SbD-QCTO approach to the synthesis of isotropic metamaterial lenses," *IEEE Antennas Wireless Propag. Lett.*, vol. 13, pp. 1783-1786, 2014.

[8] G. Oliveri, D. H. Werner, and A. Massa, "Reconfigurable electromagnetics through metamaterials - A review" *Proc. IEEE*, vol. 103, no. 7, pp. 1034-1056, Jul. 2015.

[9] G. Oliveri, E. T. Bekele, M. Salucci, and A. Massa, "Transformation electromagnetics miniaturization of sectoral and conical horn antennas," *IEEE Trans. Antennas Propag.*, vol. 64, no. 4, pp. 1508-1513, Apr. 2016.

[10] G. Oliveri, E. T. Bekele, M. Salucci, and A. Massa, "Array miniaturization through QCTO-SI metamaterial radomes," *IEEE Trans. Antennas Propag.*, vol. 63, no. 8, pp. 3465-3476, Aug. 2015.

[11] G. Oliveri, E. T. Bekele, D. H. Werner, J. P. Turpin, and A. Massa, "Generalized QCTO for metamaterial-lens-coated conformal arrays," *IEEE Trans. Antennas Propag.*, vol. 62, no. 8, pp 4089-4095, Aug. 2014.

[12] G. Oliveri, E. Bekele, M. Carlin, L. Tenuti, J. Turpin, D. H. Werner, and A. Massa, "Extended QCTO for innovative antenna system designs," IEEE Antenna Conference on Antenna Measurements and Applications (CAMA 2014), pp. 1-3, Nov. 16-19, 2014.

[13] G. Oliveri, P. Rocca, M. Salucci, E. T. Bekele, D. H. Werner, and A. Massa, "Design and synthesis of innovative metamaterial-enhanced arrays," IEEE International Symposium on Antennas Propag. (APS/URSI 2013), Orlando, Florida, USA, pp. 972 - 973, Jul. 7-12, 2013.

[14] G. Oliveri, “Improving the reliability of frequency domain simulators in the presence of homogeneous metamaterials - A preliminary numerical assessment,” *Progress In Electromagnetics Research*, vol. 122, pp. 497-518, 2012.

[15] M. Salucci, G. Oliveri, N. Anselmi, G. Gottardi, and A. Massa, "Performance enhancement of linear active electronically-scanned arrays by means of MbD-synthesized metalenses," *J. Electromagnet. Waves Appl.*, vol. 32, no. 8, pp. 927-955, 2018.

[16] M. Salucci, G. Oliveri, N. Anselmi, and A. Massa, “Material-by-design synthesis of conformal miniaturized linear phased arrays,” *IEEE Access* (doi: 10.1109/ACCESS.2018.2833199).